GENERAL ATOMIC

DIVISION OF

GENERAL DYNAMICS

JOHN JAY HOPKINS LABORATORY FOR PURE AND APPLIED SCIENCE

P.O. BOX 608, SAN DIEGO, CALIFORNIA 92112

GACD-6844
(11-31-65)

Copy No.

Technical Summary Report

EXPERIMENTAL ELECTRON SHIELDING STUDIES

Work done by:

W. Brouwer
W. Hunter
C. Jupiter
G. Merkel
J. Perez

Report written by:

C. Jupiter
G. Merkel
[redacted]

During the period of this report the following "reportable items," as defined by Article XII "Reporting of New Technology," evolved:

NONE

Project 447
NASA, George C. Marshall Space Flight Center
Huntsville, Alabama
Contract Number NAS 8-11304

November 26, 1965

CONTENTS

FIGURES

PREFACE

During the last 30 years the passage of electrons through matter, i.e., multiple scattering and energy straggling, has been considered by many workers.[1-3] In order to make possible an analytical treatment of multiple scattering or energy straggling, the theoretical treatment was frequently limited to thin targets which correspond to a relatively small energy loss.[4-8] Situations involving large electron energy losses frequently were considered in terms of the continuous slowing down approximation.[9-11] Even the thin target theoretical results were subject to severe restrictions. For example, the well-known work of Landau,[5] later refined by Blunk and Leisegang,[8] deals only with energy loss fluctuations and neglects deviations of the electron paths from a straight line. On the other hand, theoretical work such as that by Goudsmit and Saunderson,[4] and by Molier[6-7] describes only thin target angular distributions and neglects energy straggling.

Recently, Martin Berger[12] has developed a program for calculating thick target energy and angular distributions which is based on a combination of transport theory and Monte Carlo techniques. Since the number of interactions between the incident electrons and the thick target slab can be of the order of 10^6, it is unrealistic to attempt to model the actual physical situation in a Monte Carlo calculation. In Berger's program the trajectory of the electron through the thick slab is divided into approximately 100 steps. The behavior during each step is described by suitable multiple interaction theory. For example, the energy of an electron, after traversing a step ΔS, is determined by the Blunk-Leisegang energy distribution, whereas the direction of the electron is determined by the Goudsmit-Saunderson distribution.

R. Scalettar at General Atomic is now developing a purely transport theoretical approach to the passage of electrons through thick targets which will consider both energy straggling and angular distributions.

At present there are many problems that arise in electron shielding work which cannot be adequately answered by existing multiple scattering theories. This is especially true in regard to space vehicles.

The electron shielding problem in space is quite complex with regard to both the source characteristics and the interaction of electrons with shielding materials. High intensities of electrons with energies less than 0.5 MeV have been observed in the region of the earth's magnetic field; these electrons may be stopped by relatively thin walls, and their efficiency for conversion to bremsstrahlung during the stopping process is small. However, more energetic electrons also present in the earth's field present a serious shielding problem because of their high penetrability and higher efficiency for the production of bremsstrahlung and secondary electrons. Naturally occurring higher-energy electrons may also be present in the trapping zones about the earth. Experiments have shown that large numbers of electrons with energies up to about 10 MeV may be injected into the trapping zones of the earth's magnetic field by the detonation of a nuclear device a few hundred miles above the earth's surface. The lifetime of these electrons appears to be rather indefinite, depending considerably upon "dumping" mechanisms such as magnetic storms. The intensity of electrons trapped during the 1962 Starfish experiment was considered sufficiently high to present a radiation hazard for space vehicles and their contents.

In the work described in this report, thick target energy straggling and angular distributions are compared to Berger's calculations. The measurements presented here are in general agreement with Berger's Monte Carlo calculations, except that the measured spectra have a wider energy distribution than the Monte Carlo results. The broader experimental measurements are to be expected since straggling due to bremsstrahlung was not considered in Berger's calculations.

I. SUMMARY

The first twelve-month period (6/29/64-8/31/65) of the experimental portion of the Electron Shielding Studies Program under NASA contract NAS 8-11304 has been completed. The experimental apparatus for measuring the electron penetration through thick slabs and for measuring the production of bremsstrahlung in thick slabs has been designed and assembled.

The energy and angular spectra of electrons produced by the passage of 8.2 and 4.0 MeV electrons through various thick aluminum targets have been measured and compared to Monte Carlo calculations performed by M. J. Berger of the National Bureau of Standards. A number of bremsstrahlung spectra measurements at 8.0 and 4.0 MeV have also been obtained.

The design of a scattering chamber which will be the principal component in an experimental system to measure electron single interaction cross sections and single interaction bremsstrahlung production in thin targets has been completed. The present experimental setup allowed measurements using thick targets for electron and bremsstrahlung spectrum measurements for emission angles between 0 and 45 degrees. The new scattering chamber will allow an extension of these measurements to both thick and thin target electron and bremsstrahlung spectra for emission angles between 0 and 165 degrees.

II. DESCRIPTION OF THE LINAC FACILITY AND ELECTRON SHIELDING APPARATUS

2.1 GENERAL DISCUSSION

The work described in this report was performed at the General Atomic Linear Accelerator (Linac) facility in San Diego, California.

Figure 1 is a plan drawing of the Linac facility showing the relative locations of the Accelerator, the Linac Control Room, the Data Taking Room, and the Experimental Room. The bulk of the electron shielding experimental apparatus is located in the area labeled Experimental Room, whereas most of the electronics instrumentation used in the measurements are located in the Data Taking Room. The General Atomic Linac is capable

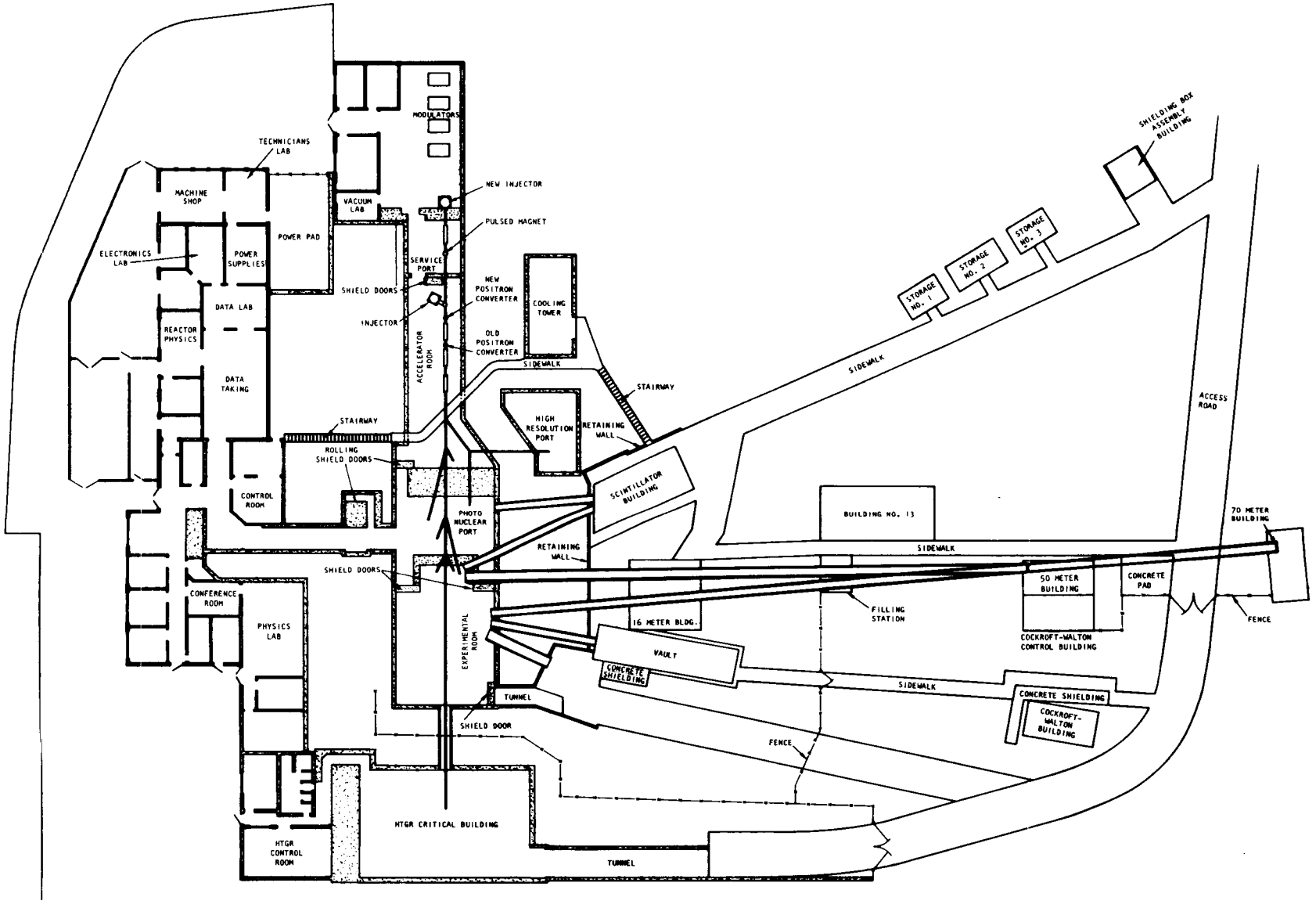

Fig. 1--Schematic plan of Linear Accelerator Facility

of producing electron beams with electron energies ranging from less than 1 MeV up to 45 MeV. The machine can also accelerate positrons with energies from less than 1 MeV to energies as high as 30 MeV.

Figure 2 is a detailed schematic plan showing the experimental electron shielding apparatus orientation. As is shown in Fig. 2 electrons from the Linac enter the system through the water-cooled collimator (1) which confines the electron beam to a horizontal and vertical dimension of 0.2 inch. A matched pair of beam translation magnets (2) and (3) then deflect the electron beam to an angle of 15 degrees, perform an energy analysis and place the electron beam in a parallel pencil of rays at the center of the target chamber (7). A second collimator (4) is appreciably larger than the beam size and is designed to remove background radiation streaming down the vacuum pipe. The Faraday cup (5) may be remotely retracted out of the beam by using an air piston. The target changer (6) consists of a remotely controlled rotating assembly carrying different targets plus a blank which is positioned at the center of the target chamber (7). This chamber is a flexible bellows rotatable in the horizontal plane through 45 degrees. The entire detection system consisting of the secondary electron analysis magnet (8), the gamma ray spectrometer (9) and the electron detector (10) is mounted on a rigid support and rotates about the center of the target chamber. The gamma ray spectrometer consists of a 5-inch diameter, 6-inch long NaI(Tl) crystal, housed in a thick lead shield. The electron detector employs a thin scintillator observed by a photomultiplier tube.

Figure 3 is a more detailed schematic of a portion of the electron shielding apparatus. The apparatus as shown here has been positioned to measure electron and bremsstrahlung spectra at an angle θ to the direction of the incident beam. An illustration of the retractable Faraday cup and of the rotating target assembly which allows the experimenter to change targets is also shown.

2.2 ANALYZING AND TRANSLATION MAGNETS

The matched pair of magnets labeled (2) and (3) in Fig. 2 are the principal components of an achromatic beam translation system of the type described by K. L. Brown.[13] If the electron analyzing magnet, labeled (8) in Fig. 2, is positioned to 0 degrees as shown in that figure and if the rotating target holder is positioned to correspond to a "target-out position", magnet (8) can be used to analyze the translated beam.

Figure 4 shows the beam spread for 7.6 MeV electrons with no analyzing slits between (2) and (3). The full-width half-maximum (FWHM) energy spread is approximately 10%. The insertion of 1/4 inch slits between (2) and (3) reduces the energy spread to approximately 2%. Figure 5

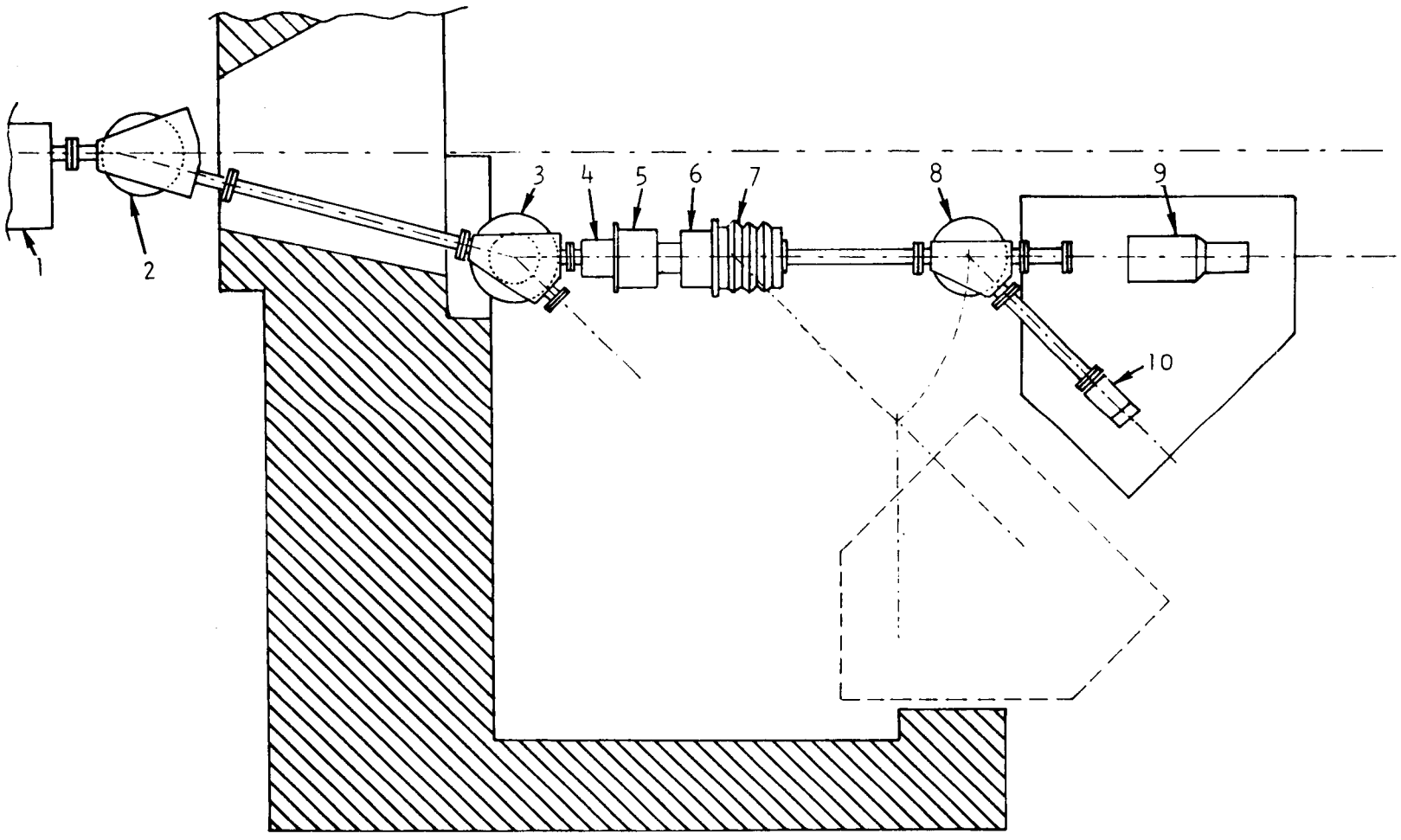

Fig. 2--Experimental arrangement for electron penetration experiments including beam analyzing and translation system: (1) collimator; (2), (3) matched pair, beam translating and energy analyzing magnets; (4), (5) Faraday cup; (6) target changer; (7) flexible (rotatable) target chamber; (8) electron spectrometer magnet; (9) NaI(Tl) crystal bremsstrahlung spectrometer; (10) NaI(Tl) electron detector.

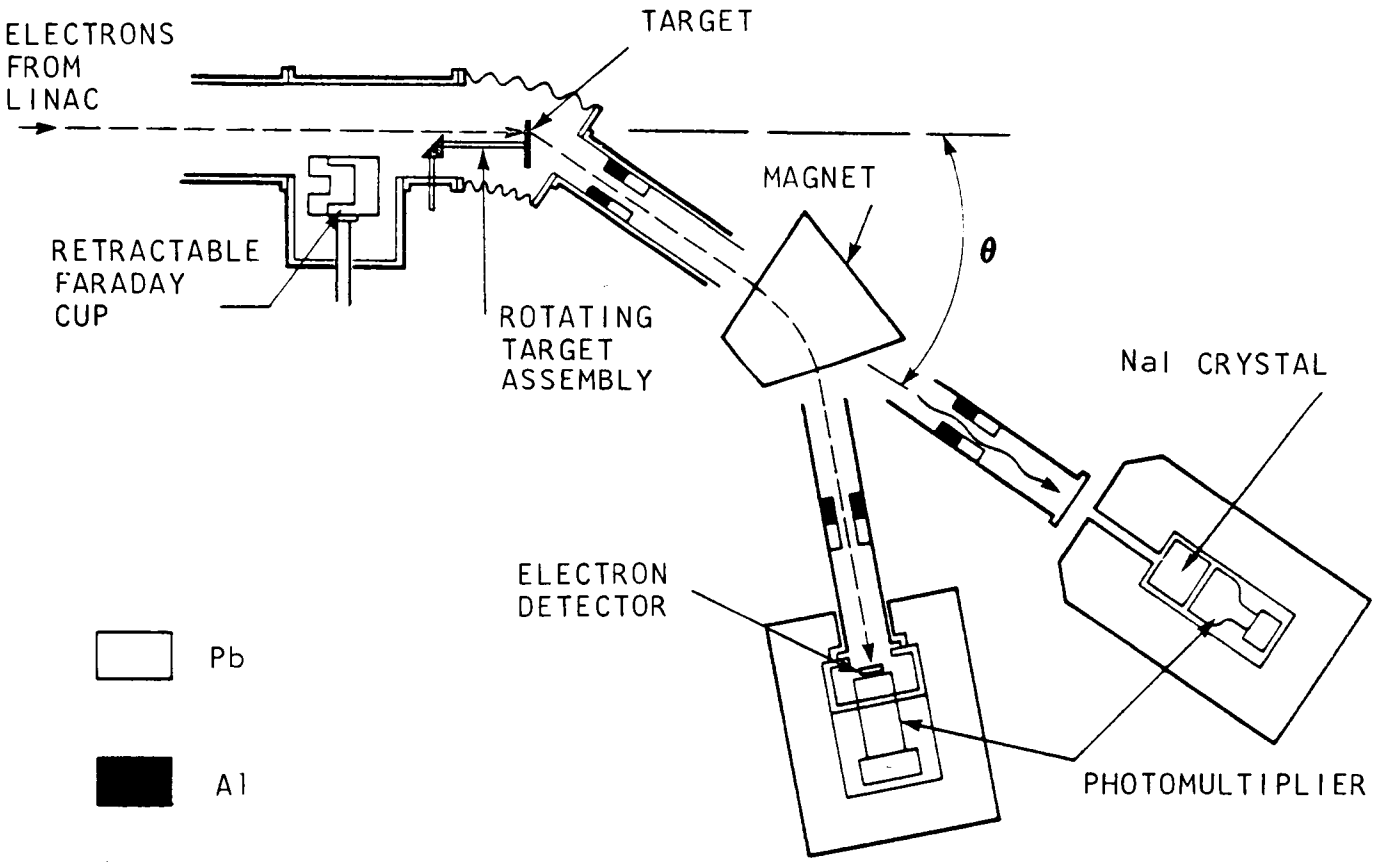

Fig 3 -- Experimental arrangement for electron penetration experiments

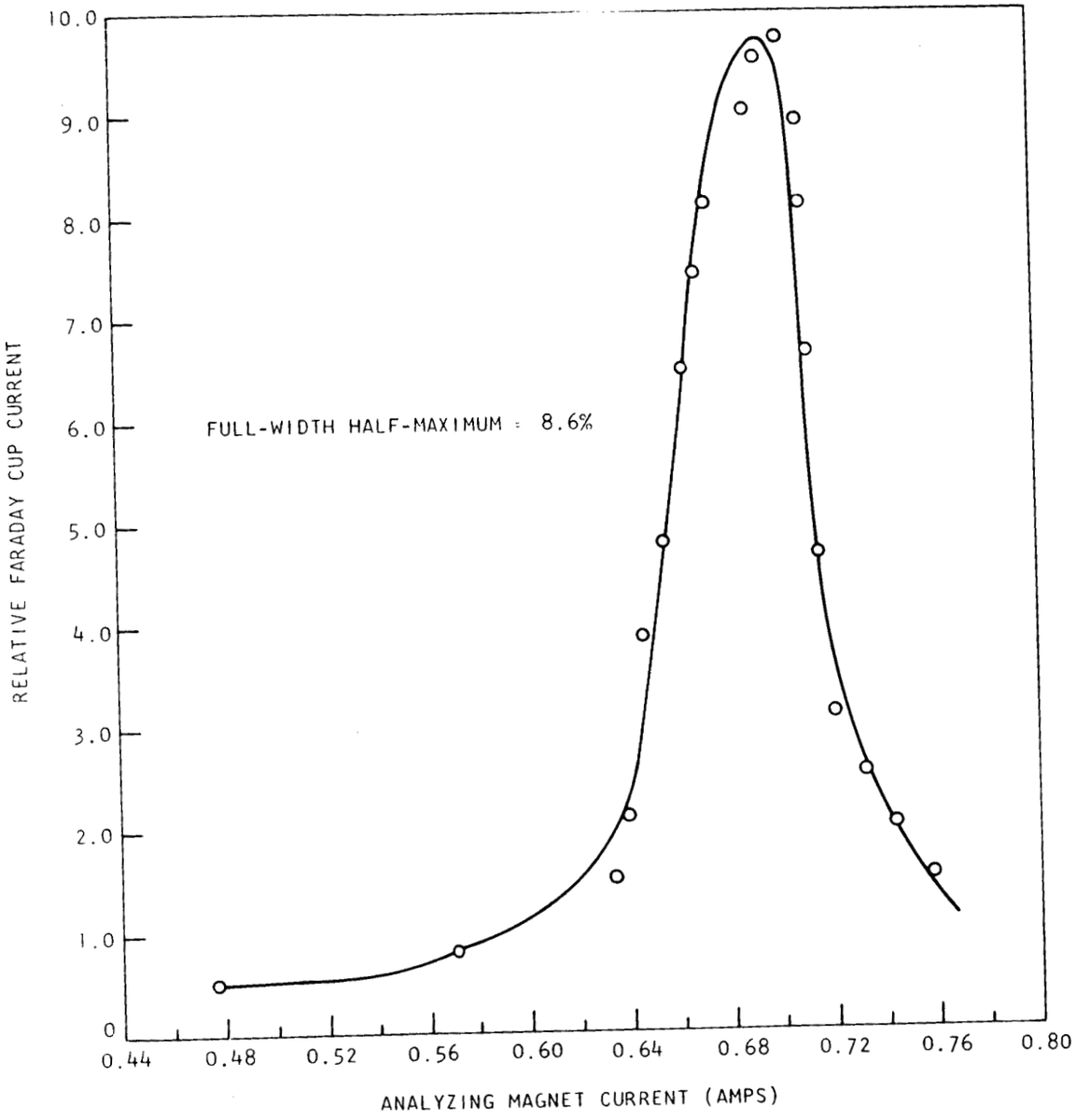

Fig. 4 -- Magnetic analysis of 7.6 MeV electron beam (no analyzing slit) FWHM = 8.6%

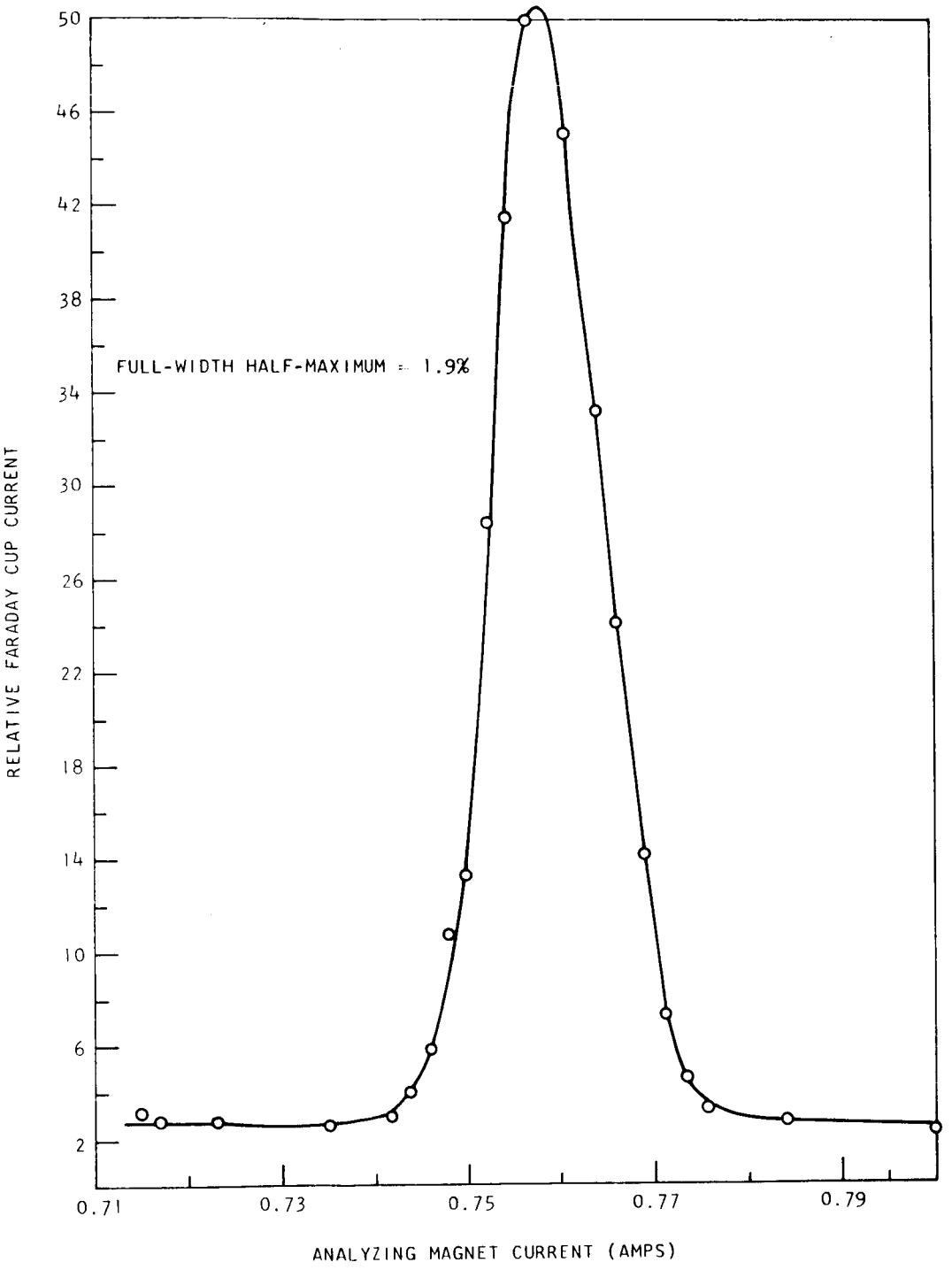

Fig. 5 -- Magnetic analysis of 8 MeV electron beam (1/4 inch analyzing slit) FWHM = 1.9%

shows the results of analyzing an 8 MeV beam after the 1/4 inch slits were installed. Figure 6 shows a similar analysis of the 5.5 MeV beam. The energy spread of the beam after passing through the matched pair of magnets could be improved to well below 1% by decreasing the analyzing width to less than 1/4 inch. (The data in Figs. 4 to 7 were obtained with a Faraday cup, rather than the NaI(Tl) electron scintillation counter shown in Figs. 2 and 3.)

III. ELECTRON SPECTROMETER

The principal components of the electron spectrometer shown in Fig. 3 are a 45-degree bending magnet[14] and an energy sensitive scintillation counter. The dashed line through the analyzing magnet represents the path of the straggled electrons. The two sets of analyzing slits placed along the electron path on both sides of the analyzing magnets are 1/4 inch wide and consist of 3 inches of aluminum followed by 3 inches of lead.

The aluminum front faces of the slits are effective in reducing the magnitude of slit scattering and Bremsstrahlung production while the lead backing absorbs most of the Bremsstrahlung produced in the aluminum. The installation of the two sets of analyzing slits resulted in target-in to target-out counting ratios as high as 10^4 to 1 at the peaks of straggled electron spectra.

The bottom half of Fig. 7 is a block diagram of the electronics associated with the electron spectrometer. The Linac trigger, which occurs in coincidence with the Linac electron burst, activates the digital delay generator which produces two pulses that, respectively, open and close the gate circuit which allows scintillation counter pulses to pass into the pulse height analyzer. The time that the gate circuit is open can be accurately measured by the time interval meter The digital delay generator is set to keep the gate circuit open for a length of time slightly longer than the Linac beam pulse length.

Figure 8 shows a pulse height distribution of the pulses produced in a 1-inch diamter 3/4-inch thick NaI(Tl) crystal scintillation counter by analyzed 4 MeV electrons. The FWHM is approximately 9%. The target-out background counting rate was essentially zero.

The electron counting system contains an inherent pulse pile-up indicating mechanism. The magnet essentially quantizes any straggled electrons that pass through the two sets of collimating slits to an energy E. Consequently any pulse pile-up results in the production of energy pulses in the scintillation counter corresponding to an energy of 2E, with an average spread ΔE of $\simeq 10\%$.

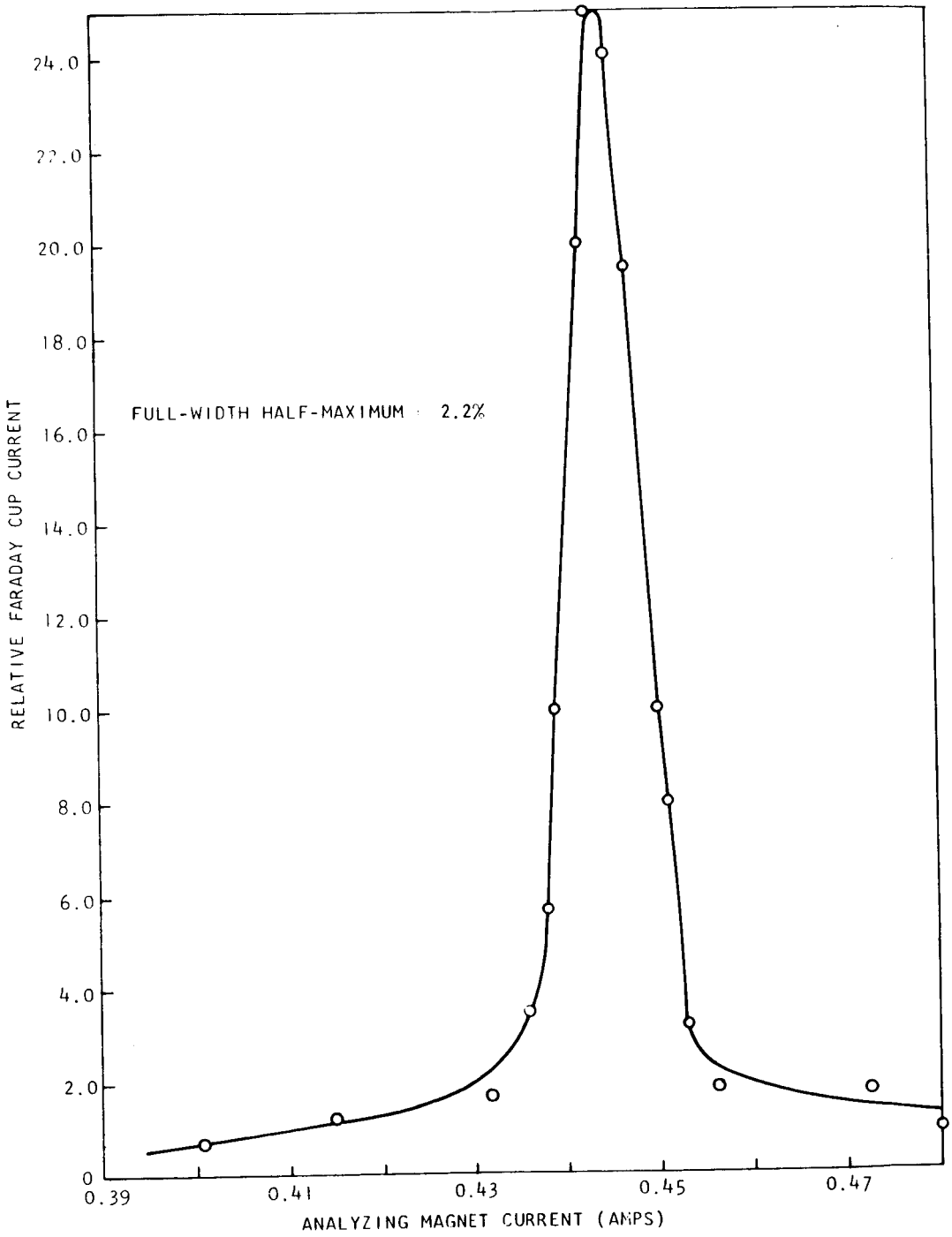

Fig. 6 -- Magnetic analysis of 5.5 MeV electron beam (1/4 inch analyzing slit) FWHM = 2.2%

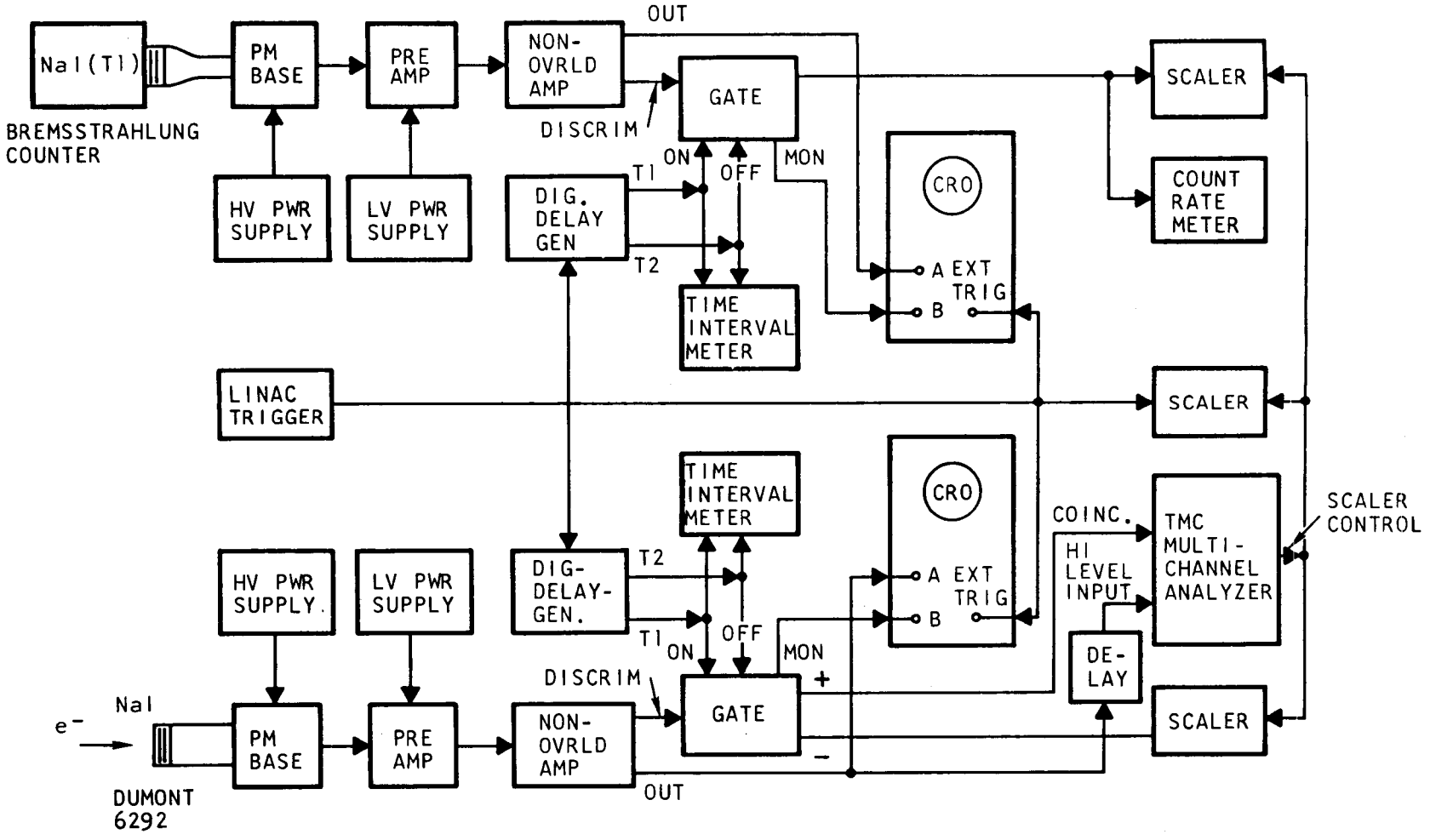

Fig. 7--Block diagram of electronics for electron spectrometer. The energy spectrum of the electrons in pulse height analyzed; the bremsstrahlung counter is used to monitor the incident beam.

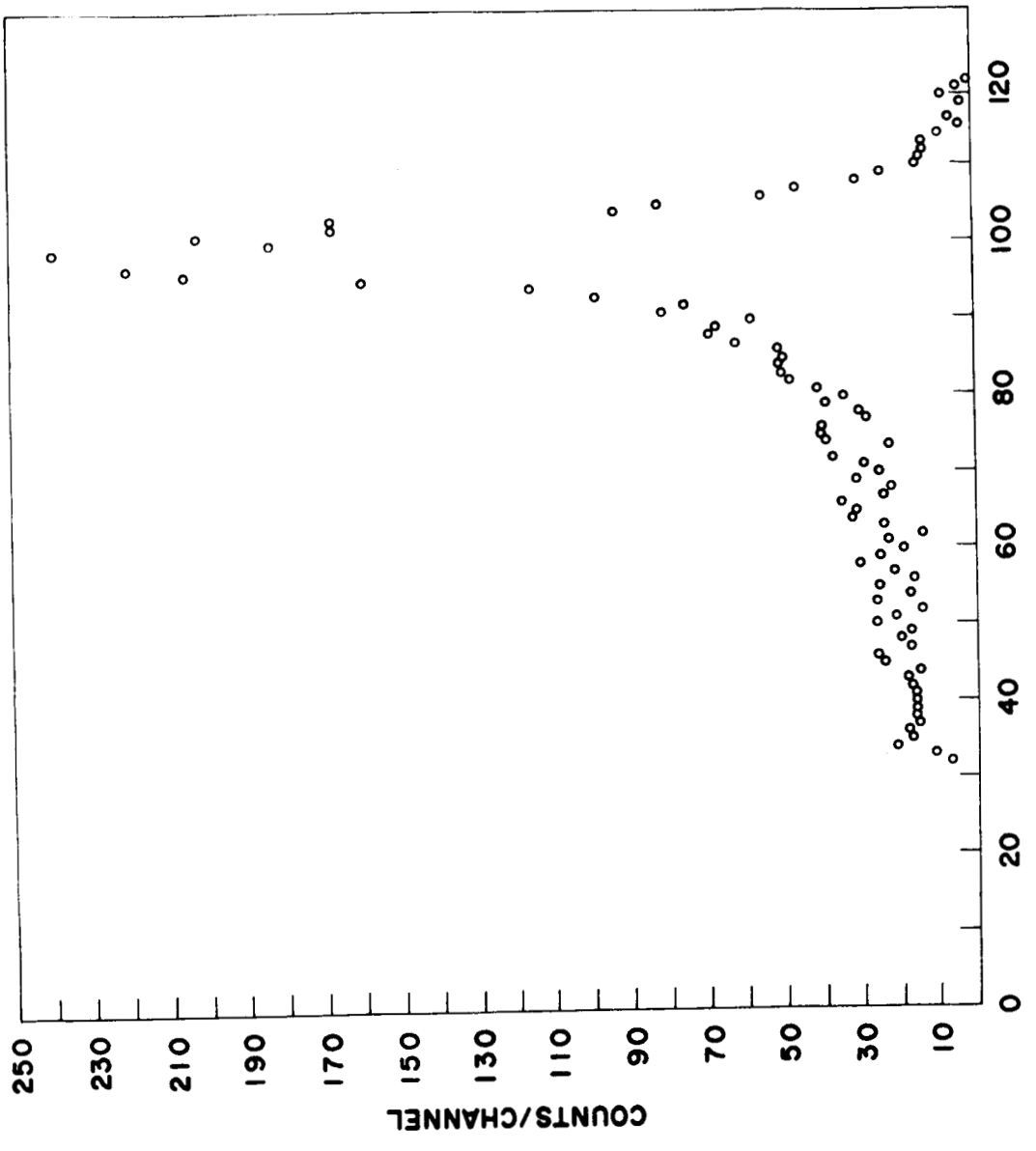

Fig. 8 -- Pulse height distribution produced by monoenergetic electrons in NaI(Tl) scintillation counter (Full width half maximum = 9%)

IV. MAGNET CALIBRATIONS

4.1 GENERAL DISCUSSION

Three completely different and independent techniques were used to obtain magnet calibrations. The matched pair of analyzing and translation magnets were calibrated using the known activation threshold for copper. The electron spectrometer magnet was calibrated using an ion source. The calibrations of the two sets of magnets were checked against each other by setting the electron spectrometer to 0 degrees and passing the unobstructed Linac beam through the two magnet systems.

The two methods mentioned above were used to initially calibrate the magnets. Since the activation technique requires the use of the LINAC, and the ion source technique requires partial dismantling of the experimental apparatus, a third simple and convenient technique using internal conversion electrons is being developed in order to recheck the calibration at later times.

4.2 MAGNETIC FIELD MEASUREMENT

The three magnets in the experimental setup are shown in Fig. 2. The matched pair of translation and analyzing magnets are connected in series to the same power supply. Therefore, only the field of the second magnet of the matched pair is measured and monitored. The field of the 45 degree electron analyzing magnet is independently measured and monitored.

The field strengths are measured with two Rawson type 822 rotating coil gaussmeters. The null balance output of these gaussmeters has an accuracy of 0.1% or ± .05 Gauss, whichever is larger.

The combined drift of the gaussmeters and the magnet power supplies, over a 24-hour period, has been found to be less than 1%.

4.3 ACTIVATION CALIBRATION OF ANALYZING AND TRANSLATION MAGNETS

The relationship between electron momentum and the magnitude of the magnetic field in the matched pair of analyzing and translating magnets was established by determining the threshold of the Cu^{63} $(\gamma, n)Cu^{62}$ reaction as a function of magnetic field strength. Copper discs, 1/16-in. thick, were bombarded by the analyzed electron beam for two minutes, using various magnetic field strengths in the analyzing magnet. The electron

beam incident upon the Cu disc was integrated using a Faraday cup placed behind the Cu discs. The $Cu^{63}(\gamma, n)Cu^{62}$ threshold is 10.8 MeV.[15] The Cu^{62} nucleus decays by β^+ emission with a 9.9-minute half-life. The relative amount of activity produced in the Cu discs was determined by counting the 0.51 MeV β^+ annihilation radiation with a NaI(Tl) crystal after the Linac beam bombardment. The 9.9-minute half-life was verified by counting each disc four times for one minute, with two-minute intervals between counts.

A plot of the activity, normalized according to integrated incident current, is shown in Fig. 9. The annihilation radiation peak becomes distinct from the background at a magnet field strength of approximately 309 gauss.

4.4 ION SOURCE CALIBRATION OF 45-DEGREE ELECTRON SPECTROMETER MAGNET

A diagram of the apparatus employed in an independent atomic beam calibration of the 45-degree electron analyzing magnet is shown in Fig. 10. Thermionically emitted electrons were accelerated from the filament "f" to the grid "g" by the electron accelerating voltage AV. Atoms of the residual gases that were ionized by the accelerated electrons were then accelerated by the high voltage HV applied between the source S and the grounding electrode G. After passing through the degaussed 45-degree magnet H, the accelerated ionized atoms were first detected at the Faraday cup collectors C_2^1 C_1^1. The magnetic field was then turned on and the ionized atoms were detected at the Faraday cup collectors C_2^1 C_1^1. It was possible to scan for the various ions by either varying the magnetic field H or the accelerating voltage HV. The non-relativistic relationship between the accelerating voltage HV, the magnetic field H (gauss), the atomic ionization number Z, the ion mass M (atomic mass units), and the radius of curvature ρ (cm) is:

$$HV = \frac{(H\rho)^2 Z}{M} \quad 4,826 \times 10^{-11} \text{ volt} \qquad (1)$$

If the ionization state Z and the mass M of an ion is known, Eq. (1) can be used to obtain a very accurage value of the radius of curvature ρ. The value of the radius of curvature ρ can then be used in a relativistic equation for electrons of any energy:

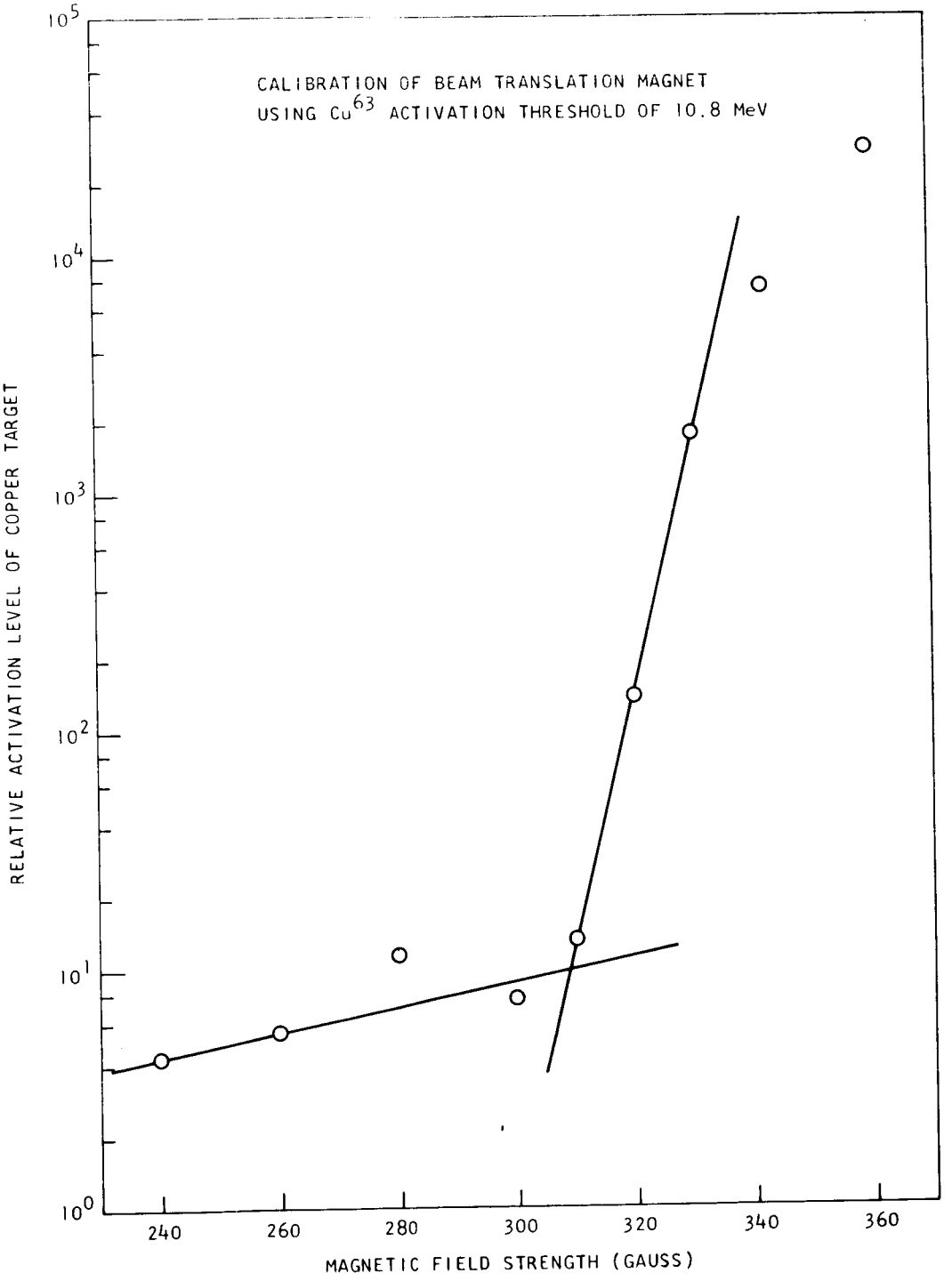

Fig. 9--$Cu^{63}(\gamma, n)Cu^{62}$ threshold calibration

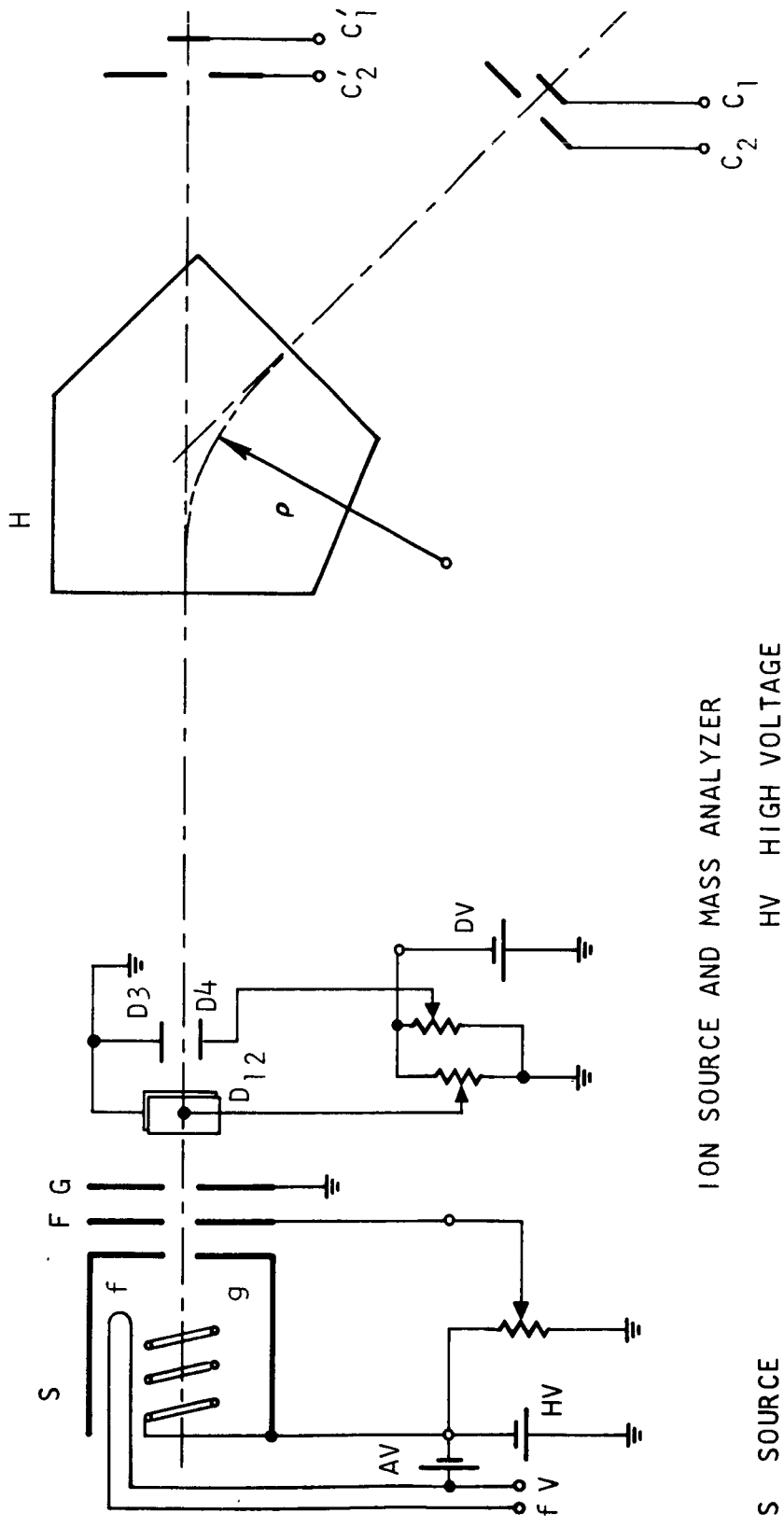

Fig. 10--Ion source apparatus

$$\left(\frac{E}{.511}\right)^2 + 1 = \left(\frac{H\rho}{1704}\right)^2 + 1 \qquad (2)$$

where E is the electron kinetic energy in MeV.

Table 1 gives the values of HV and H that correspond to peak Faraday cup readings. The assumptions about the charge states of the various ions are based on the independent threshold measurements discussed in Section 4.3. The Faraday cup current maxima attributed to the acceleration of argon, neon, or krypton only occurred after the specific gas was bled into the vacuum system. Graphs of Eq. (2) calculated with the value of ρ determined by the measurements summarized in Table 1 are shown in Figs. 11 and 12.

4.5 CALIBRATION OF ANALYZER MAGNET WITH INTERNAL CONVERSION ELECTRONS

A thin 10 millicurie Cs^{137} source has been mounted on the target holder to serve as a convenient magnet calibration device. Approximately 92% of the Cs^{137} beta decays to the 0.662 MeV metastable state of Ba^{137}. The internal conversion coefficient of this 0.662 MeV level is approximately 9.8%.[16] An absolute determination of the strength of the Cs^{137} source will, therefore, yield an independent spectrometer solid angle determination as well as an energy calibration.

V. STRAGGLED ELECTRON SPECTRUM MEASUREMENTS

The electron spectrometer described in Section III has been used to measure the energy distribution of electrons produced when an incident beam of 8.2 MeV electrons is normally incident on a 0.35-in. or 2.4-gm/cm^2 aluminum target. The measured straggled electron spectra obtained at 0, 10, 20, 30, and 40 degrees are presented in Figs. 13 to 17. The 8.2 MeV experimental measurements have been arbitrarily normalized to 24 electron counts per MeV/steradian.

The electron spectrometer has also been used to measure various straggled electron spectra for 4.0 MeV incident electrons. Figures 18 to 22 show the measured straggled spectra at 0, 10, 20, 30, and 40 degrees for 4.0 MeV electrons normally incident upon a 181-in. or 1.24-gm/cm^2 aluminum target. All of the 4.0 MeV experimental curves have been arbitrarily normalized to a maximum value of 200 electron counts per MeV/steradian. Figures 23 to 25 show the measured straggled electron spectra at 0, 20, and 40 degrees for 4.0 MeV electrons normally incident upon a .072-in. or .595-gm/cm^2 aluminum target. Finally, Fig. 26 shows the

Table 1

HV (volts)	H (gauss)	H^2/HV (gauss/volts)	A/Z	Ion Species
3500	326	30.4	1.0	H^+
1432	206	29.6	1.0	
1765	325	60.0	2.0	H_2^+
1804	328	59.8	2.0	He^{++}
2718	908	304	10.1	Ne^{++}
2735	907	301	10.0	20
2713	901	299	9.9	
2768	910	299	9.9	
2727	909	304	10.1	
2700	905	304	10.1	
2695	908	306	10.1	
2713	901	290	9.6	
2735	907	303	10.1	
2495	909	331	11.0	Ne^{++}
2494	910	332	11.0	22
2466	900	328	10.8	
2500	908	331	11.0	
2466	900	328	10.8	
2465	908	334	11.1	
2500	910	332	11.0	
1268	908	652	21.7	Ne^+
1278	910	648	21.6	22
1409	912	590	19.6	$^{20}Ne+$
1400	910	592	19.7	
1387	908	596	19.8	$^{40}Ar++$
1380	1320	1260	42.0	$^{84}Kr++$
699	1320	2490	83.0	$^{84}Kr+$
1395	1310	1230	41	Ar^+
1375	1318	1260	42.0	Kr^{++}
1375	1318	1260	42.0	
1369	1318	1270	42.3	
1367	1317	1272	42.4	
1351	1317	1285	42.8	
1350	1307	1265	42.2	

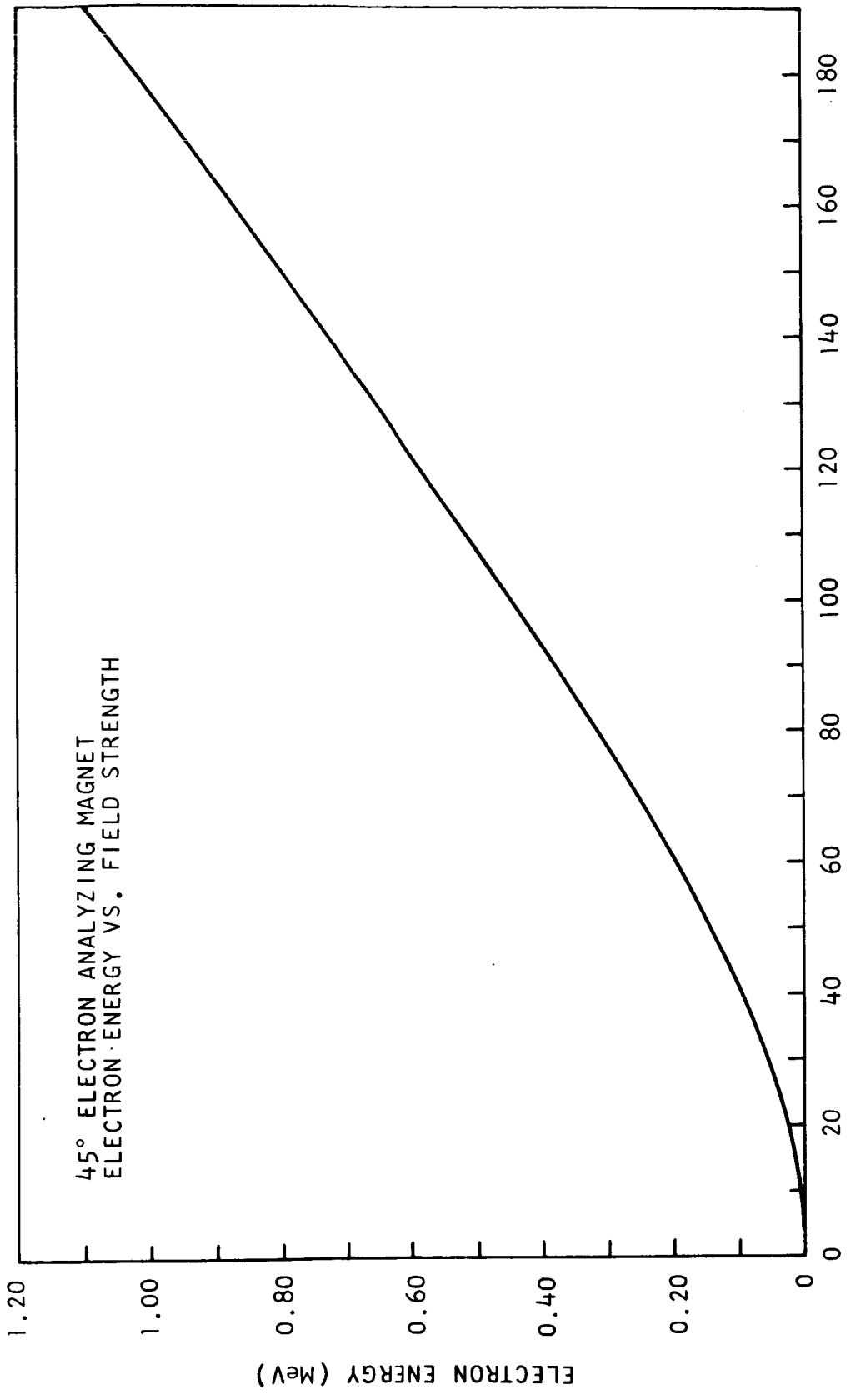

Fig. 11--Electron energy versus 45 degree spectrometer magnetic field strength

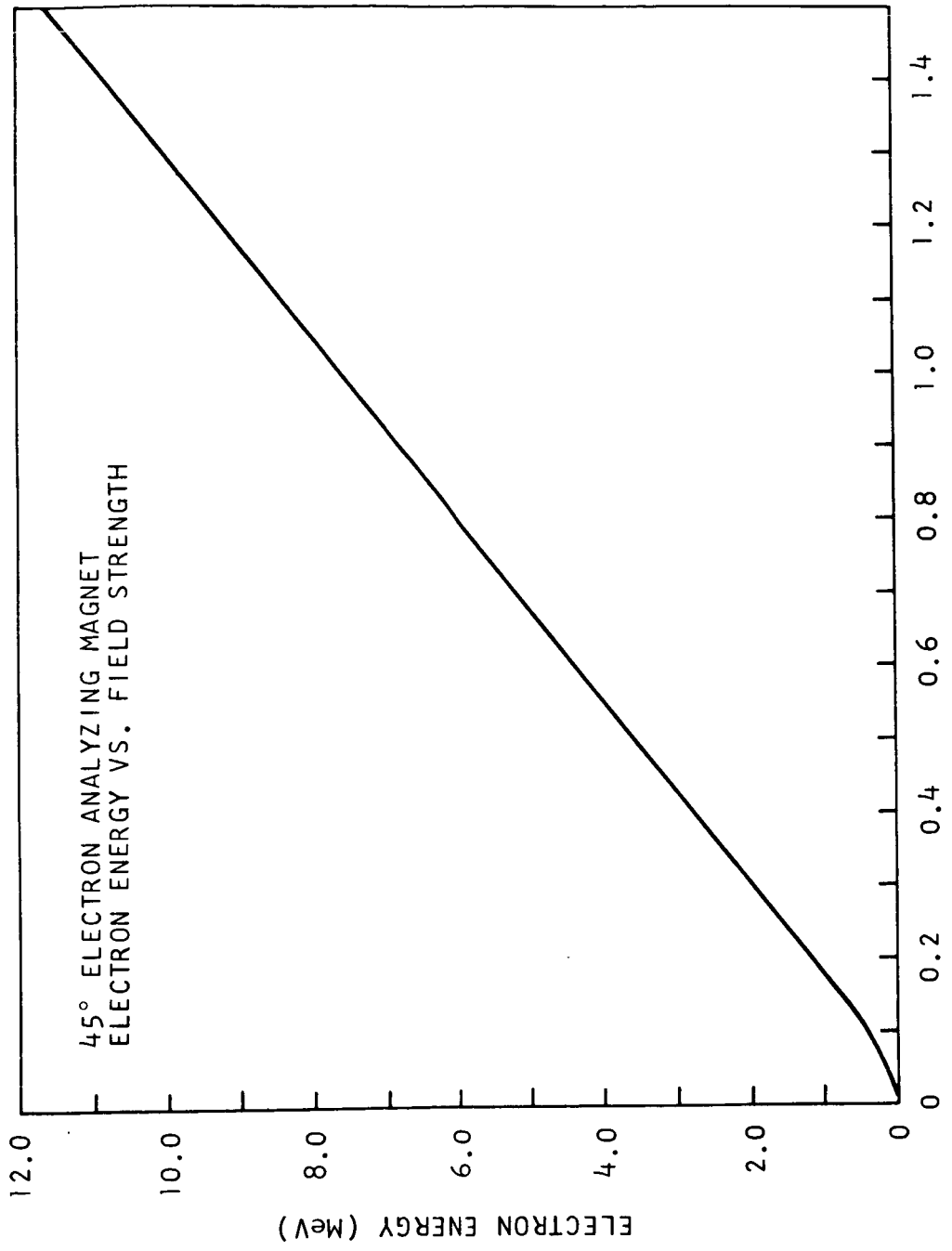

Fig. 12--Electron energy versus 45 degree spectrometer magnetic field strength

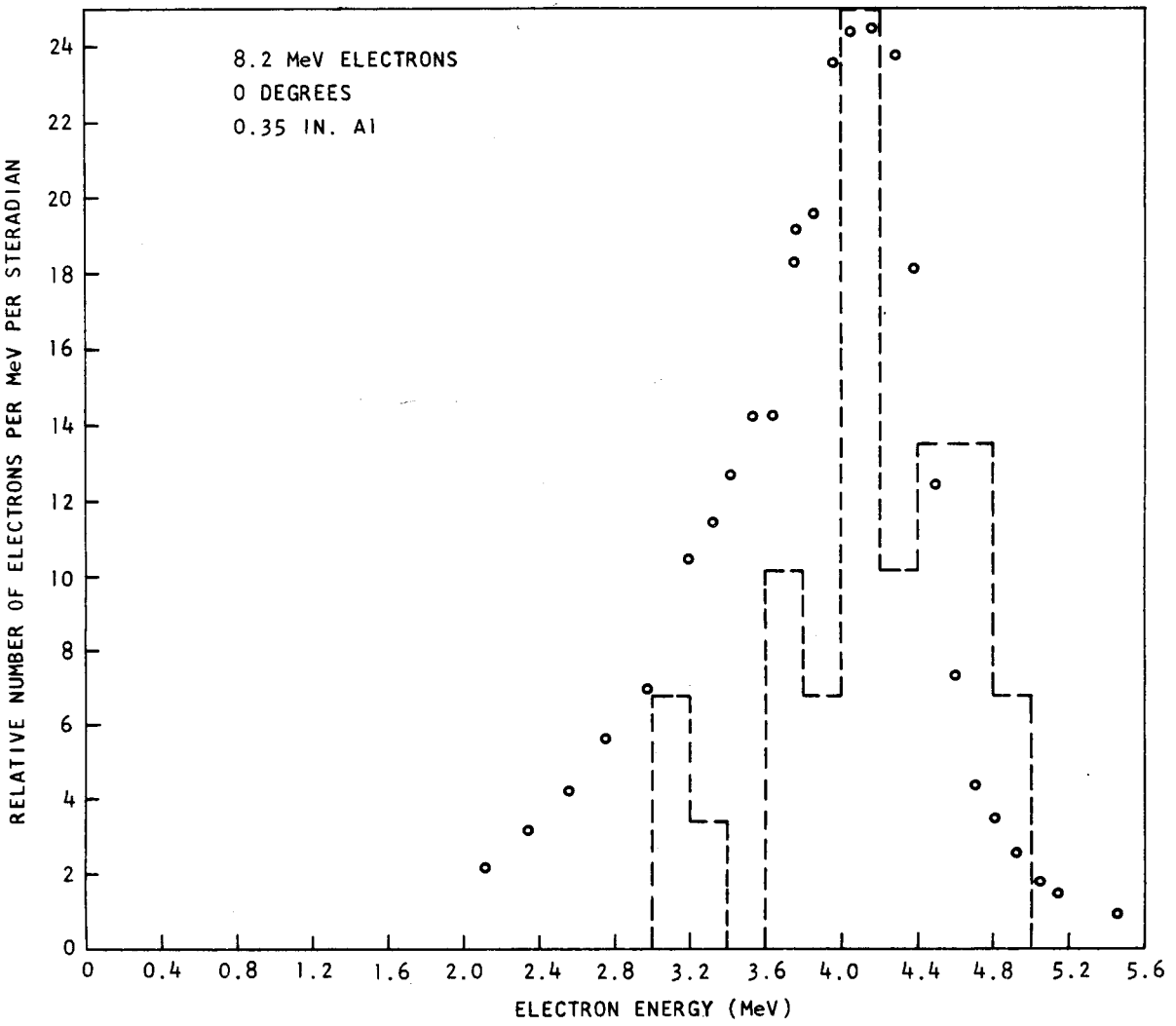

Fig. 13--Electron energy spectrum at zero degrees. The histogram corresponds to Berger's Monte Carlo calculation for the energy distribution of electrons emitted between 0 and 5 degrees.

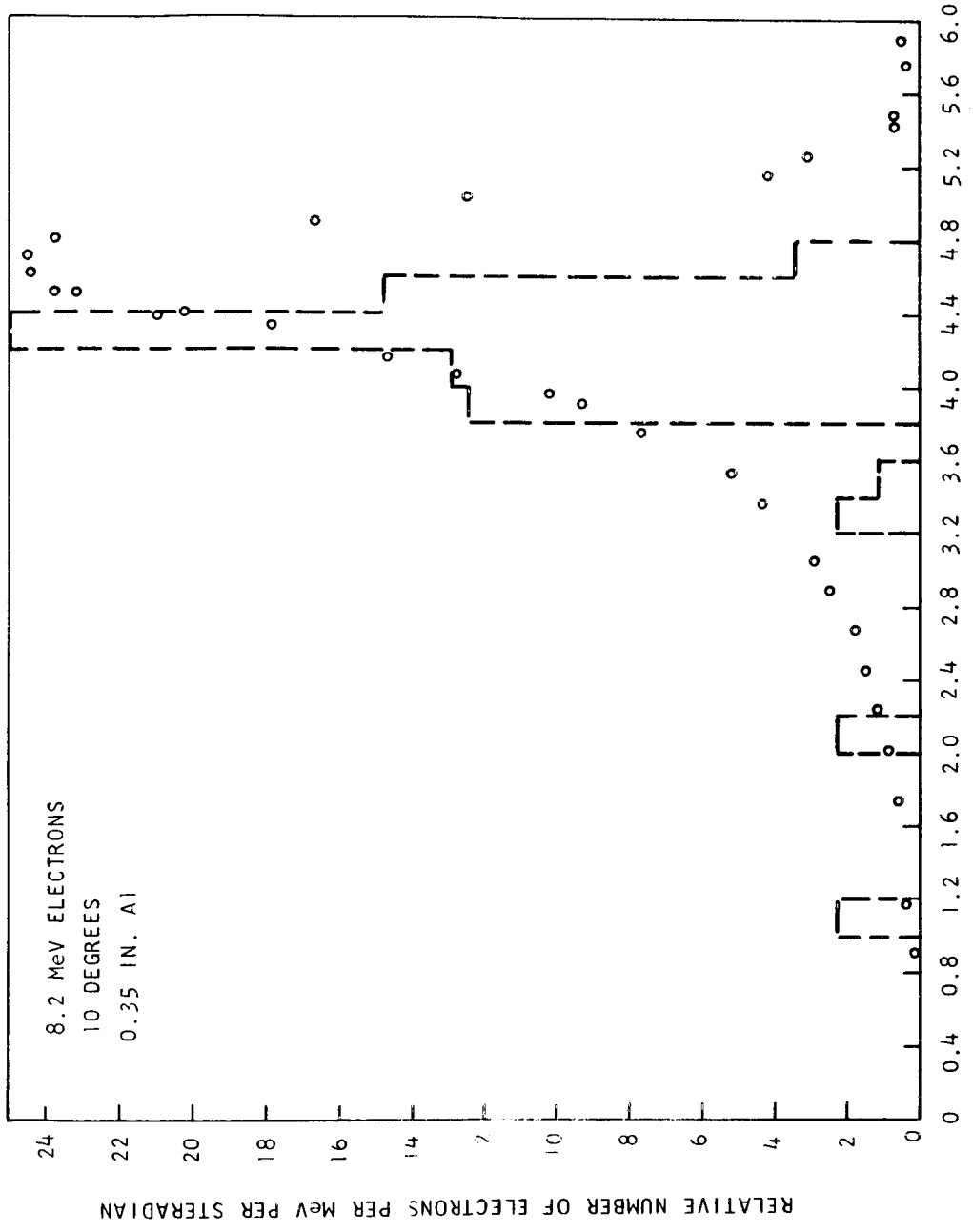

Fig. 14--Electron energy spectrum at 10 degrees. The histogram corresponds to Berger's Monte Carlo calculation for the energy distribution of electrons emitted between 5 and 10 degrees.

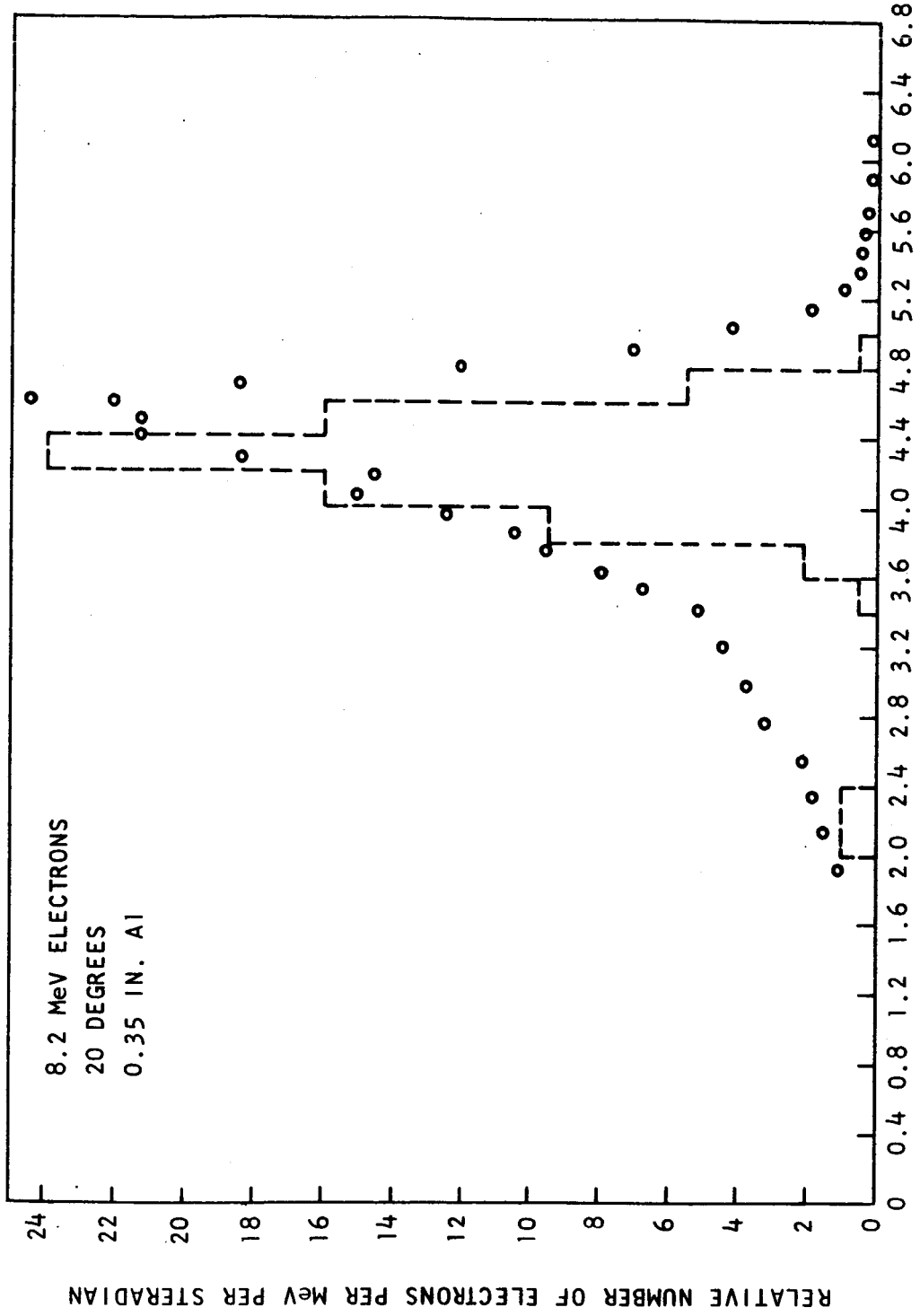

Fig. 15--Electron energy spectrum at 20 degrees. The histogram corresponds to Berger's Monte Carlo calculation for the energy distribution of electrons emitted between 15 and 20 degrees.

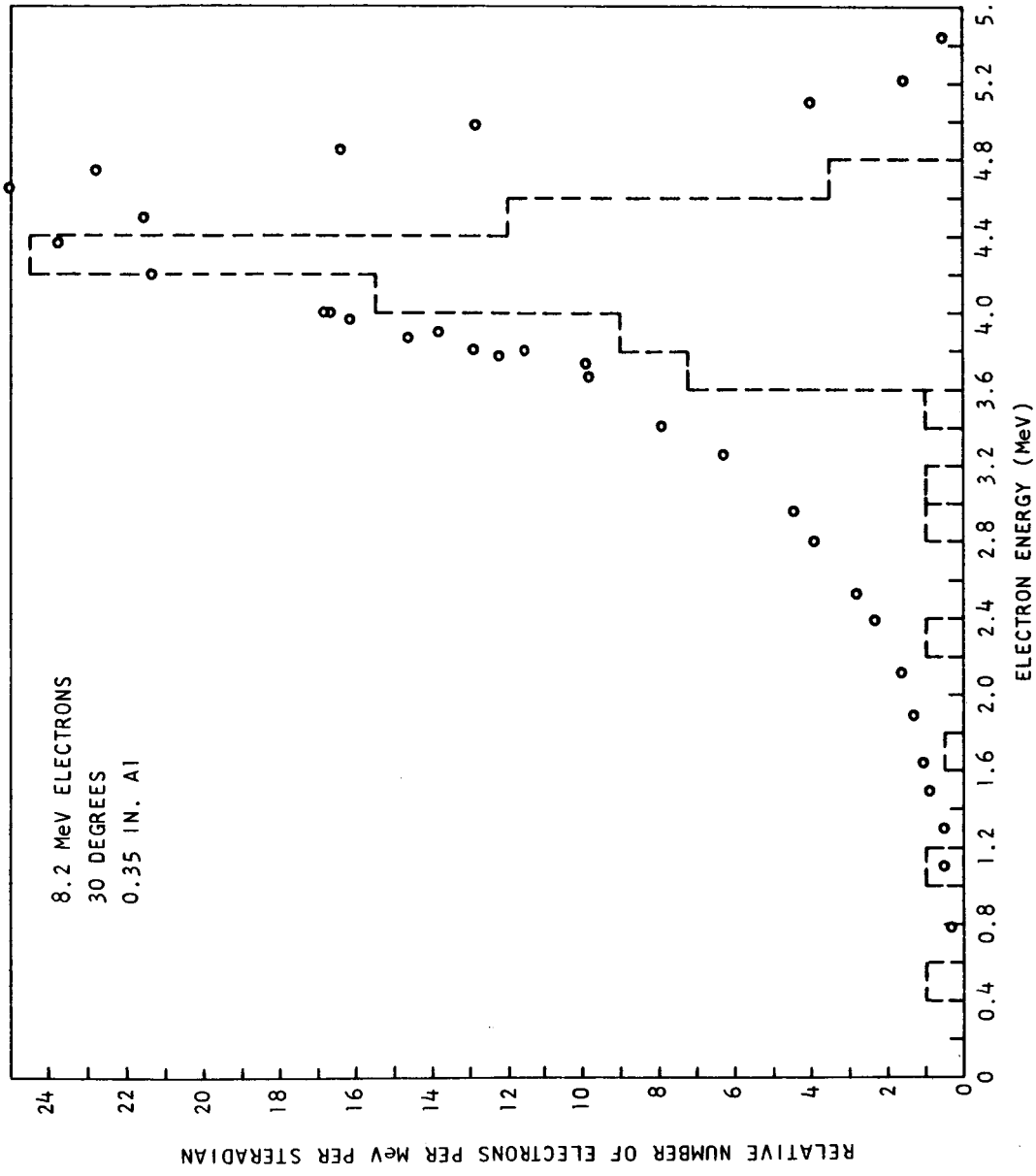

Fig. 16--Electron energy spectrum at 30 degrees. The histogram corresponds to Berger's Monte Carlo calculation for the energy distribution of electrons emitted between 25 and 30 degrees.

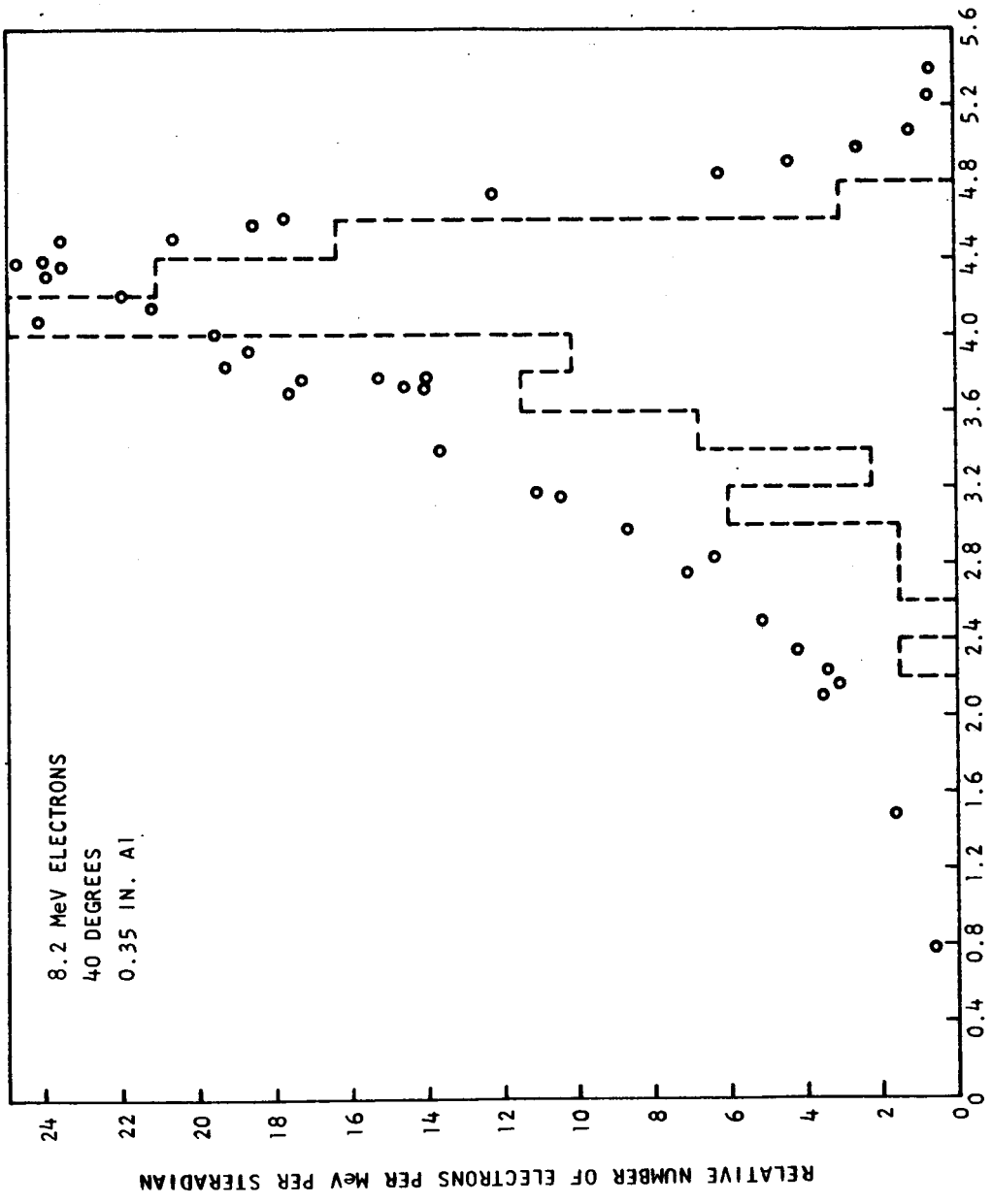

Fig. 17--Electron energy spectrum at 40 degrees. The histogram corresponds to Berger's Monte Carlo calculation for the energy distribution of electrons emitted between 35 and 40 degrees.

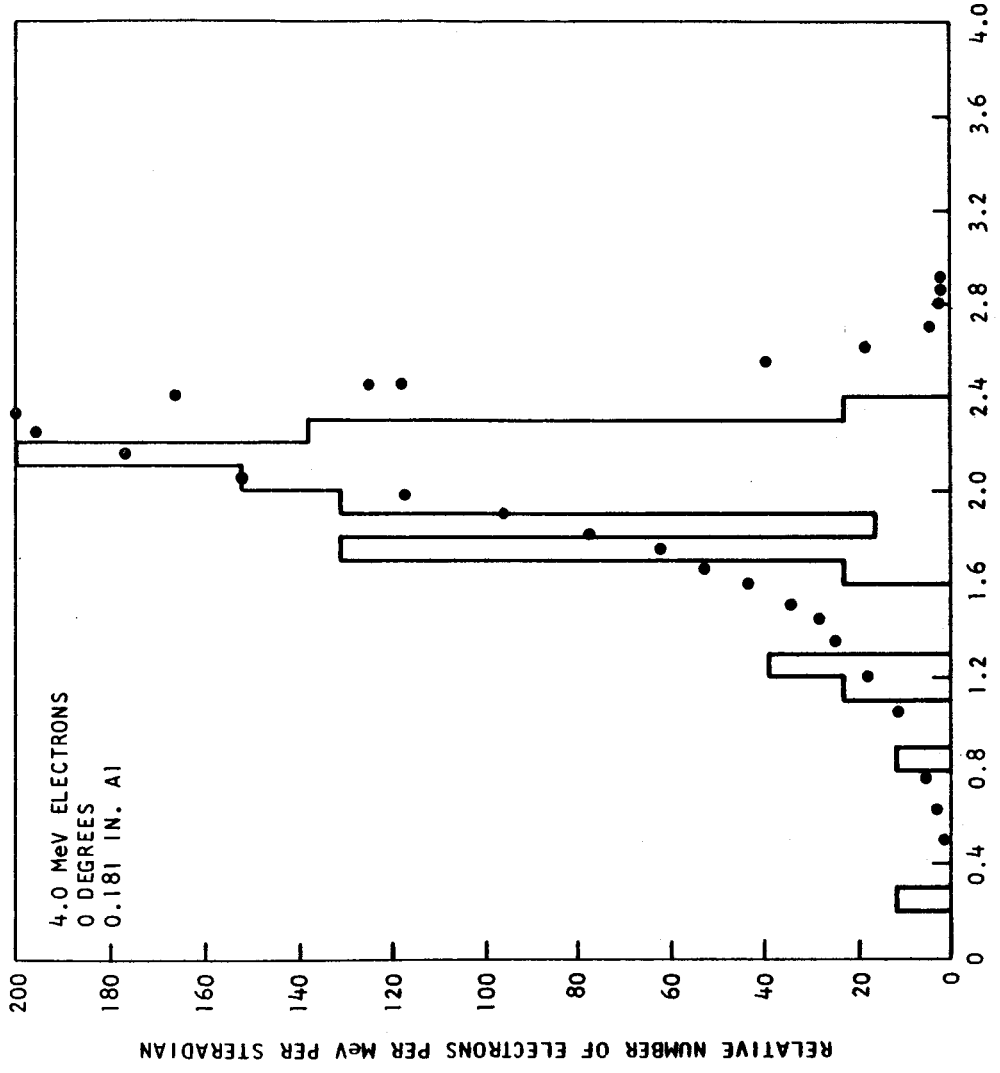

Fig. 18--Electron energy spectrum at zero degrees. The histogram corresponds to Berger's Monte Carlo calculation for the energy distribution of electrons emitted between 0 and 10 degrees. The target consists of a 0.181 in. thick aluminum slab.

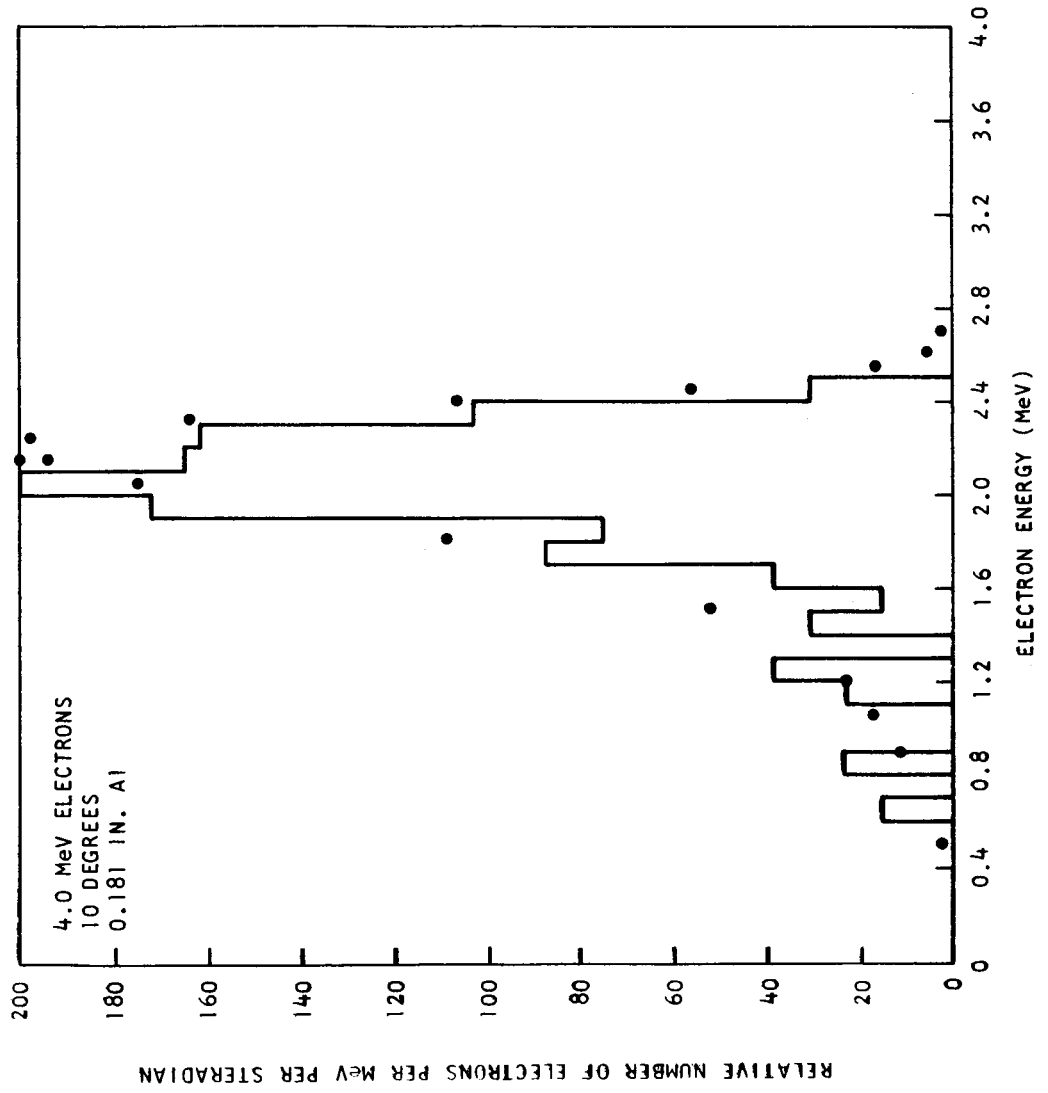

Fig. 19--Electron energy spectrum at 10 degrees. The histogram corresponds to Berger's Monte Carlo calculation for the energy distribution of electrons emitted between 5 and 15 degrees. The target consists of a 0.181 in. thick aluminum slab.

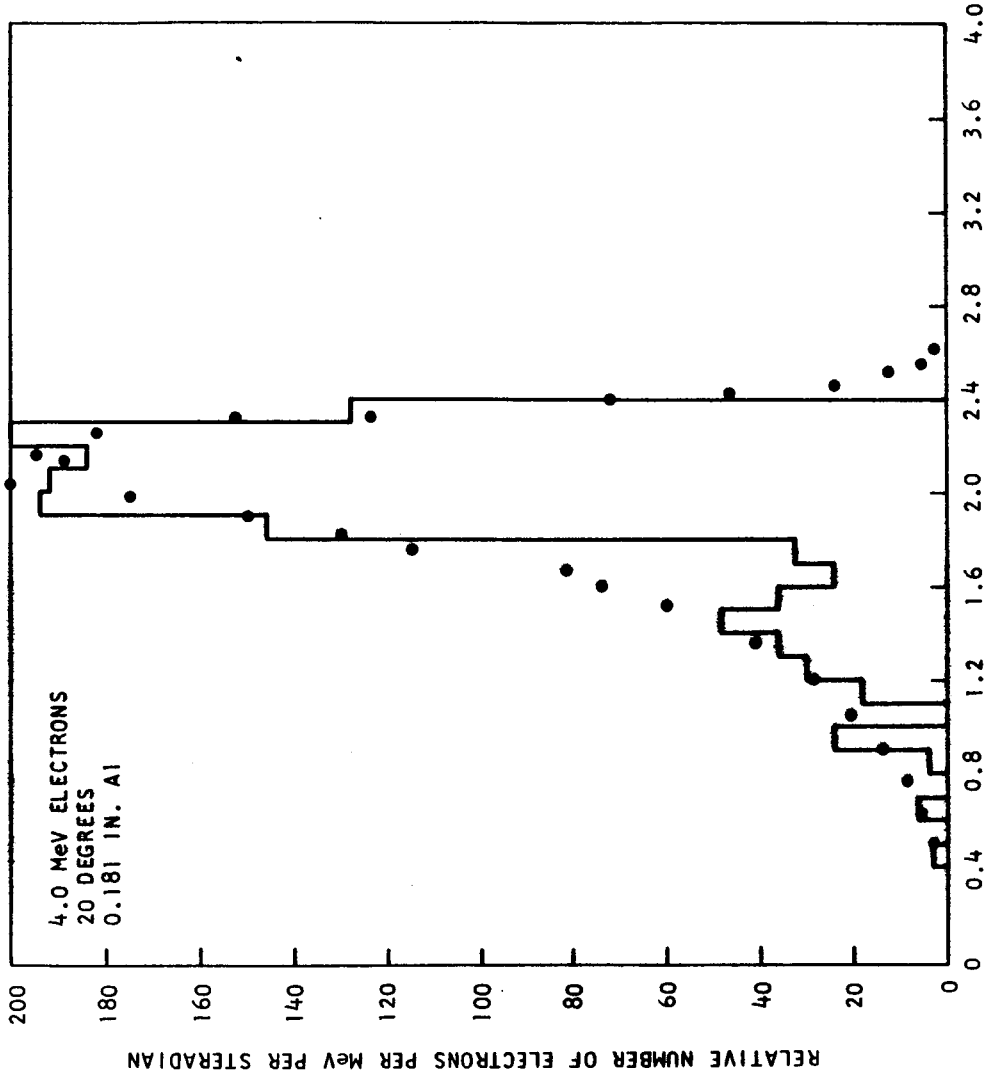

Fig. 20--Electron energy spectrum at 20 degrees. The histogram corresponds to Berger's Monte Carlo calculation for the energy distribution of electrons emitted between 15 and 25 degrees. The target consists of 0.181 in. thick aluminum slab.

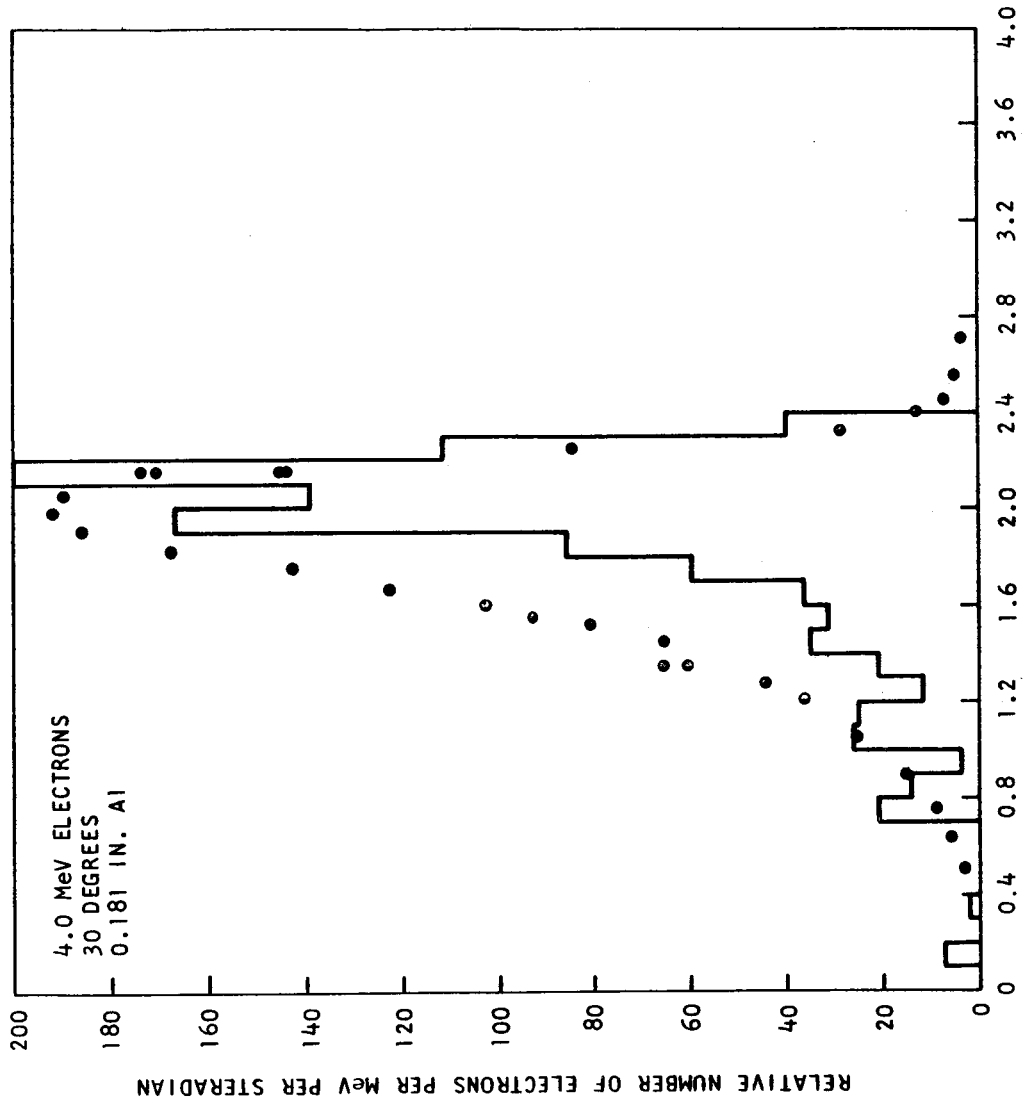

Fig. 21--Electron energy spectrum at 30 degrees. The histogram corresponds to Berger's Monte Carlo calculation for the energy distribution of electrons emitted between 25 and 35 degrees. The target consists of a 0.181 in. thick aluminum slab.

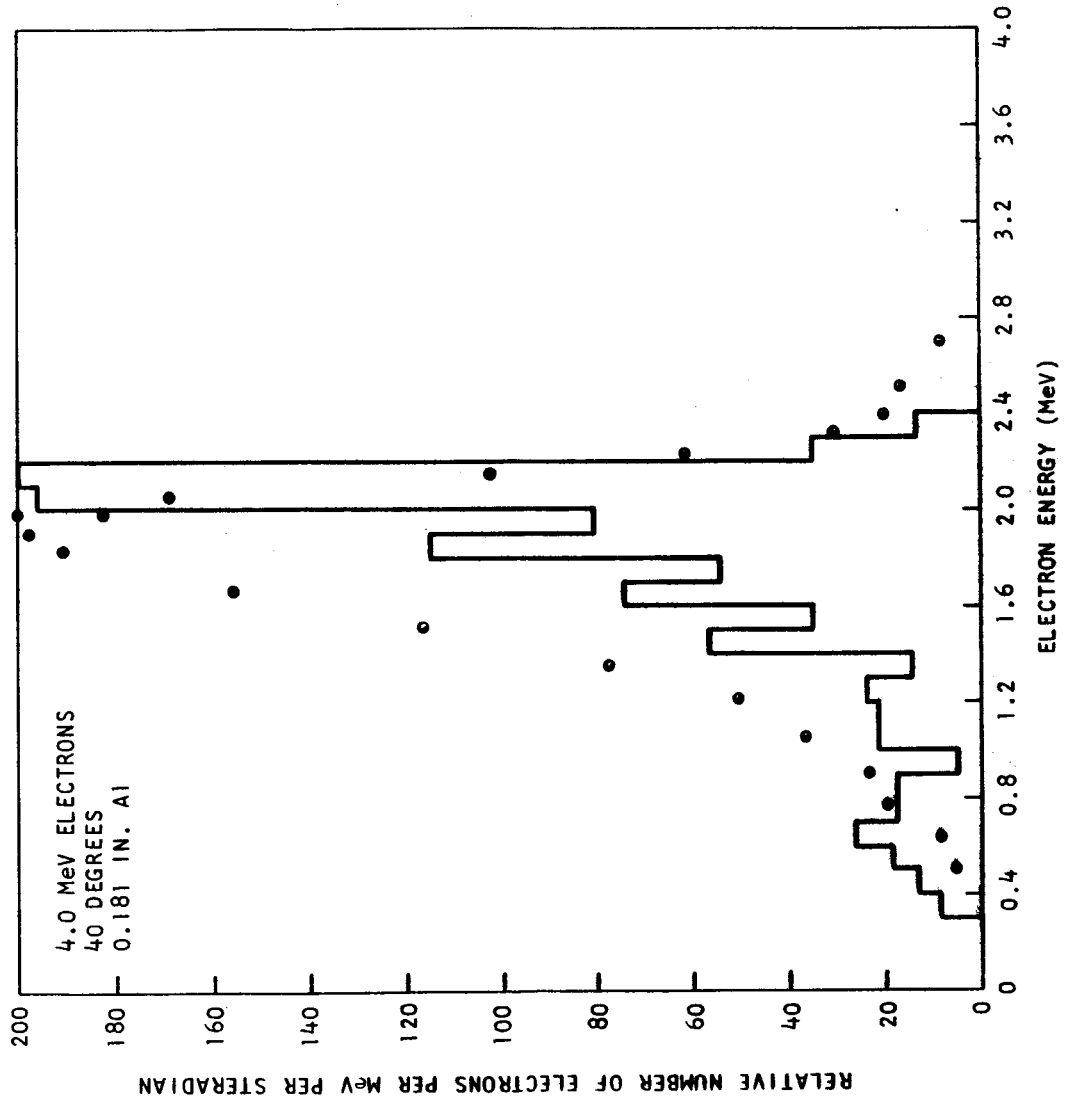

Fig. 22--Electron energy spectrum at 40 degrees. The histogram corresponds to Berger's Monte Carlo calculation for the energy distribution of electrons emitted between 35 and 45 degrees. The target consists of a 0.181 in. thick aluminum slab.

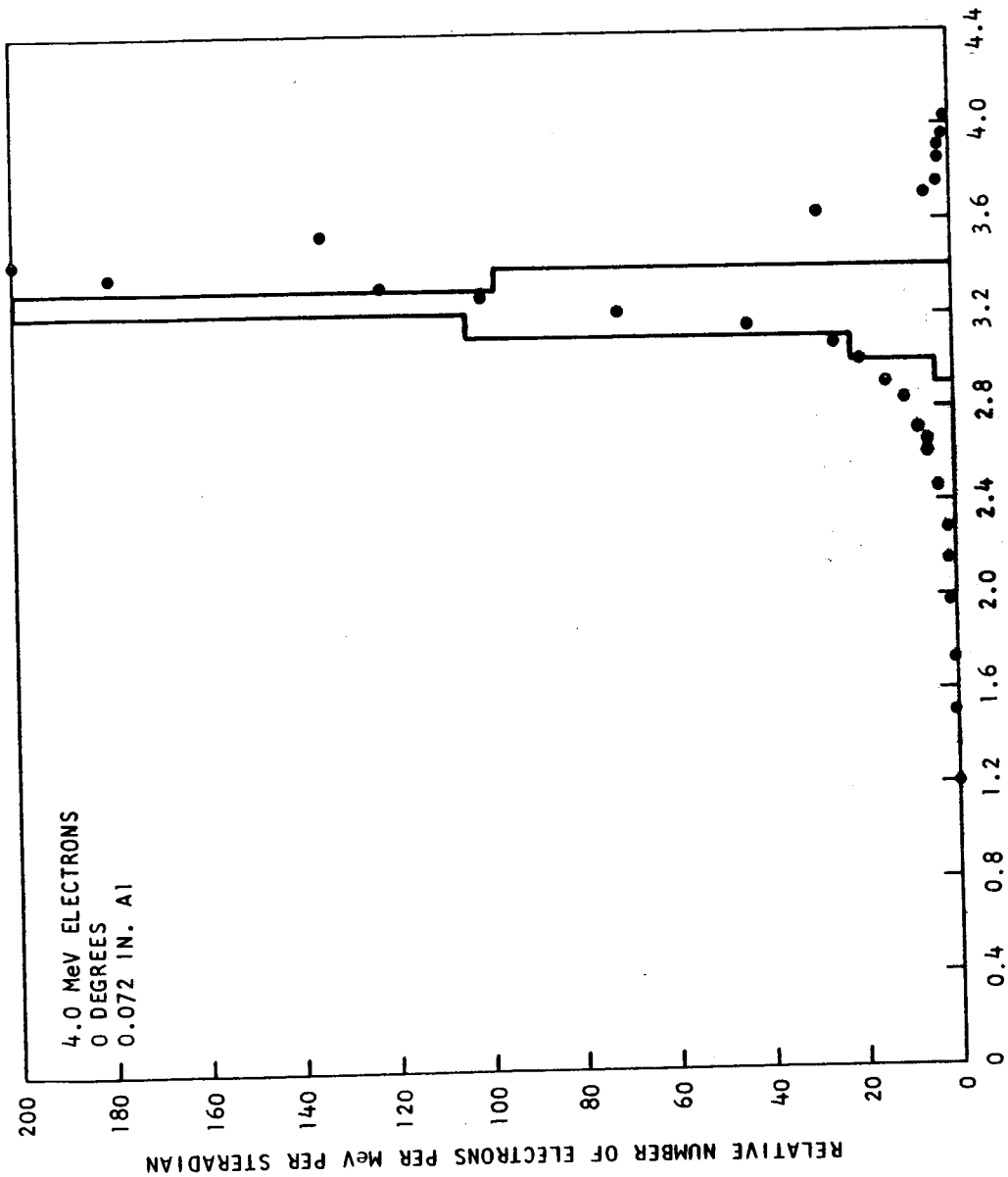

Fig. 23--Electron energy spectrum at zero degrees. The histogram corresponds to Berger's Monte Carlo calculation for the energy distribution of electrons emitted between 0 and 10 degrees. The target consists of a 0.072 in. thick aluminum slab.

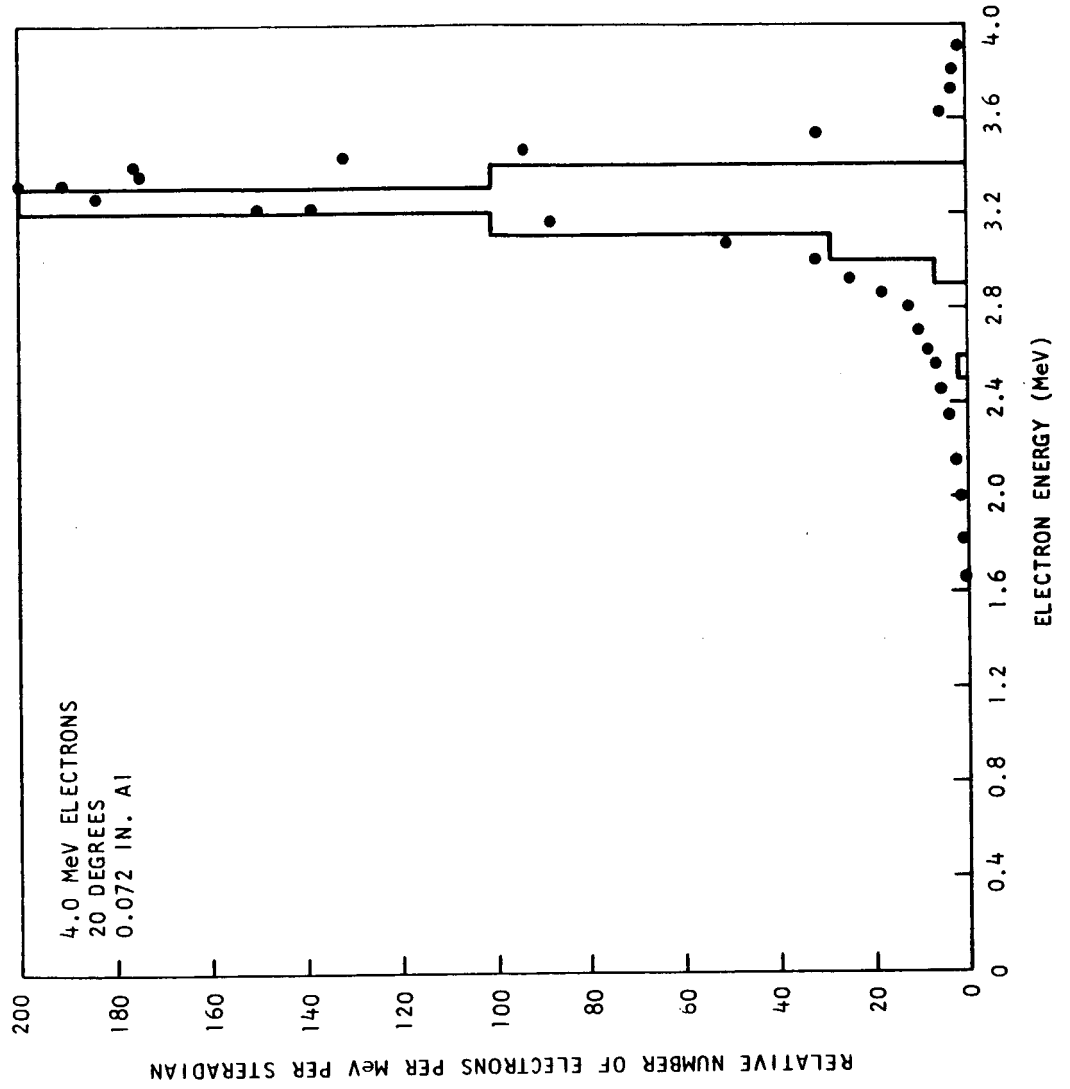

Fig. 24--Electron energy spectrum at 20 degrees. The histogram corresponds to Berger's Monte Carlo calculation for the energy distribution of electrons emitted between 15 and 25 degrees. The target consists of a 0.072 in. thick aluminum slab.

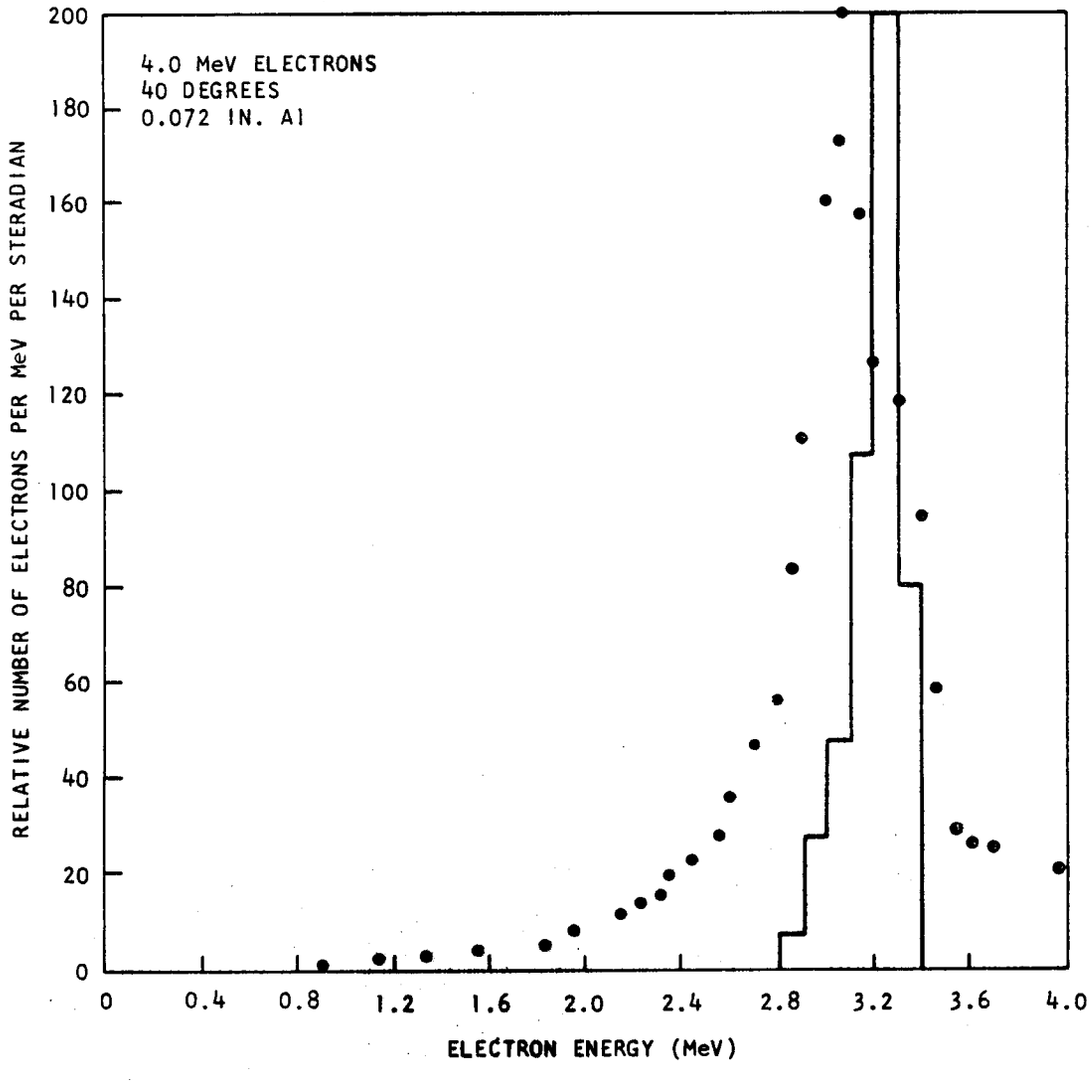

Fig. 25--Electron energy spectrum at 40 degrees. The histogram corresponds to Berger's Monte Carlo calculation for the energy distribution of electrons emitted between 35 and 40 degrees. The target consists of a 0.072 in. thick aluminum slab.

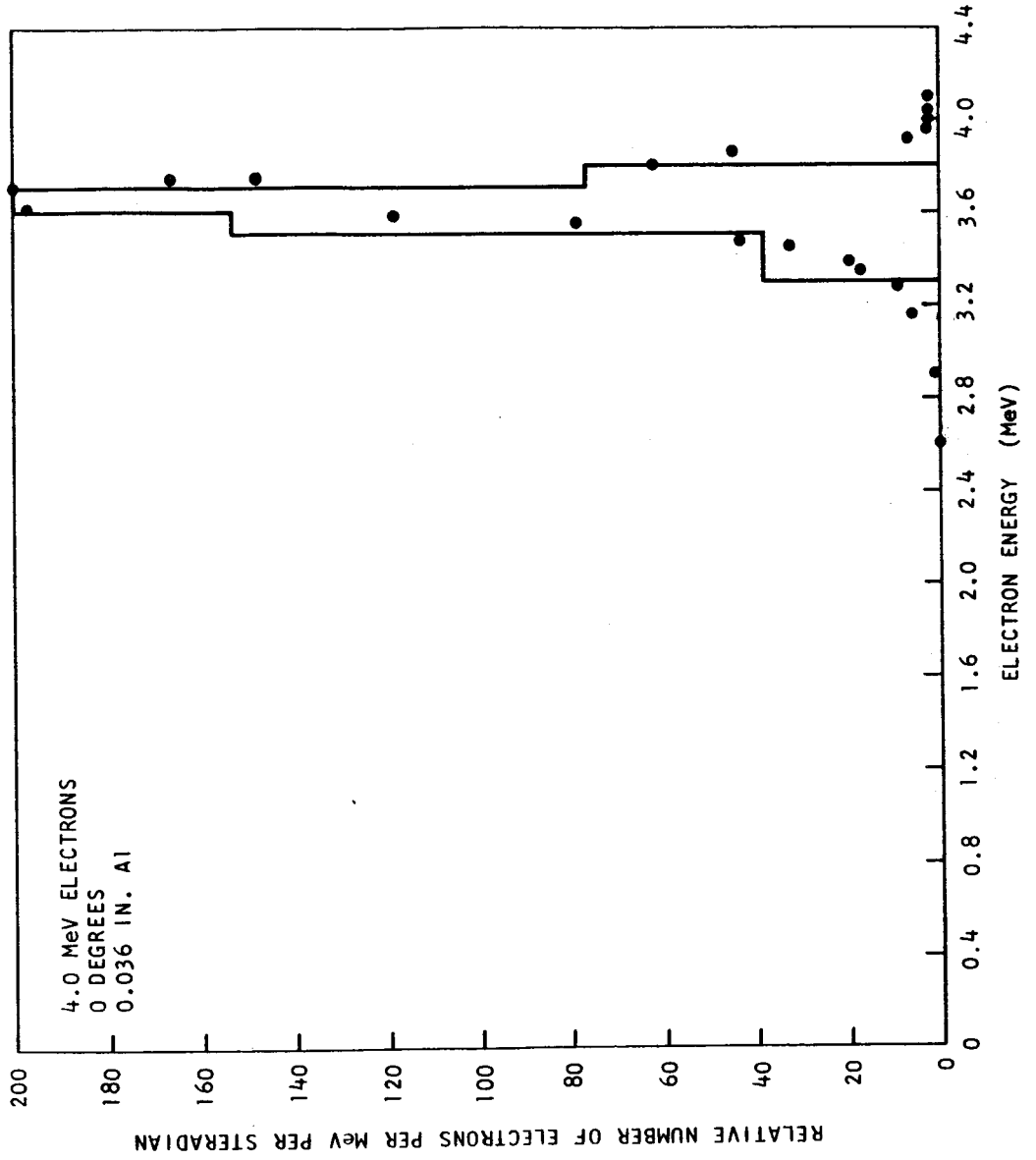

Fig. 26--Electron energy spectrum at zero degrees. The histogram corresponds to Berger's Monte Carlo calculation for the energy distribution of electrons emitted between 0 and 5 degrees. The target consists of a 0.036 in. thick aluminum slab.

measured straggled electron spectrum at 0 degrees for 4.0 MeV electrons normally incident upon a 0.036-in. or .247-g/cm^2 aluminum target.

It should be noted that none of the 8.2 MeV or 4.0 MeV experimental spectra have been corrected for the effect of the 2 % spread in the incident electron beam. This type of correction probably is unimportant in every case except the 0.247-g/cm^2 target (Fig. 26).

The measurements shown in Figs. 13 to 26 were obtained before all the problems associated with the magnet power supply regulating system and with the Rawson gaussmeter had been solved. Consequently, the scatter of experimental points is greater than the scatter would be if the measurements were made with the present improved system. Figures 27 to 28 show some recent measurements of the energy distribution of straggled electrons. As can be seen, the scatter of the measured points has been greatly reduced.

Since there can be so-called catastrophic electron-electron collisions which result in a rather large energy loss, it is of interest to measure the straggled electron spectra to as low an energy as possible. The present detection system is effective down to energies of approximately 0.1 or 0.05 MeV.

VI. COMPARISON OF ELECTRON SPECTRA WITH THE MONTE CARLO CALCULATIONS OF BERGER

Berger[12, 17] has developed a Monte Carlo code for calculating the energy and angular distributions of straggled electrons emerging from a parallel slab that is bombarded by normally incident mono-energetic electrons. The number of interactions between the incident electrons and the target slab is much too large to model the actual physical situation with the Monte Carlo calculation. In Berger's code the trajectory of the electrons through the slab is divided into approximately 100 steps. The behavior of the electrons during each step is described by suitable multiple interaction theory.

The experimental results described in Section V are compared to Berger's Monte Carlo calculations in Figs. 13 to 25. In the case of the 8.2 MeV data the Monte Carlo histograms have been arbitrarily normalized to a maximum value of 25, and in the case of the 4.0 MeV data to a maximum value of 200. The 8.2 MeV experimental curves are compared to calculations for 8.0 MeV incident electrons. The 8.0 MeV Monte Carlo calculations have been extrapolated to 8.2 MeV by shifting the theoretical curves 0.2 MeV in the positive direction. The 4.0 MeV measurements have been compared to calculations for 4.0 MeV incident electrons.

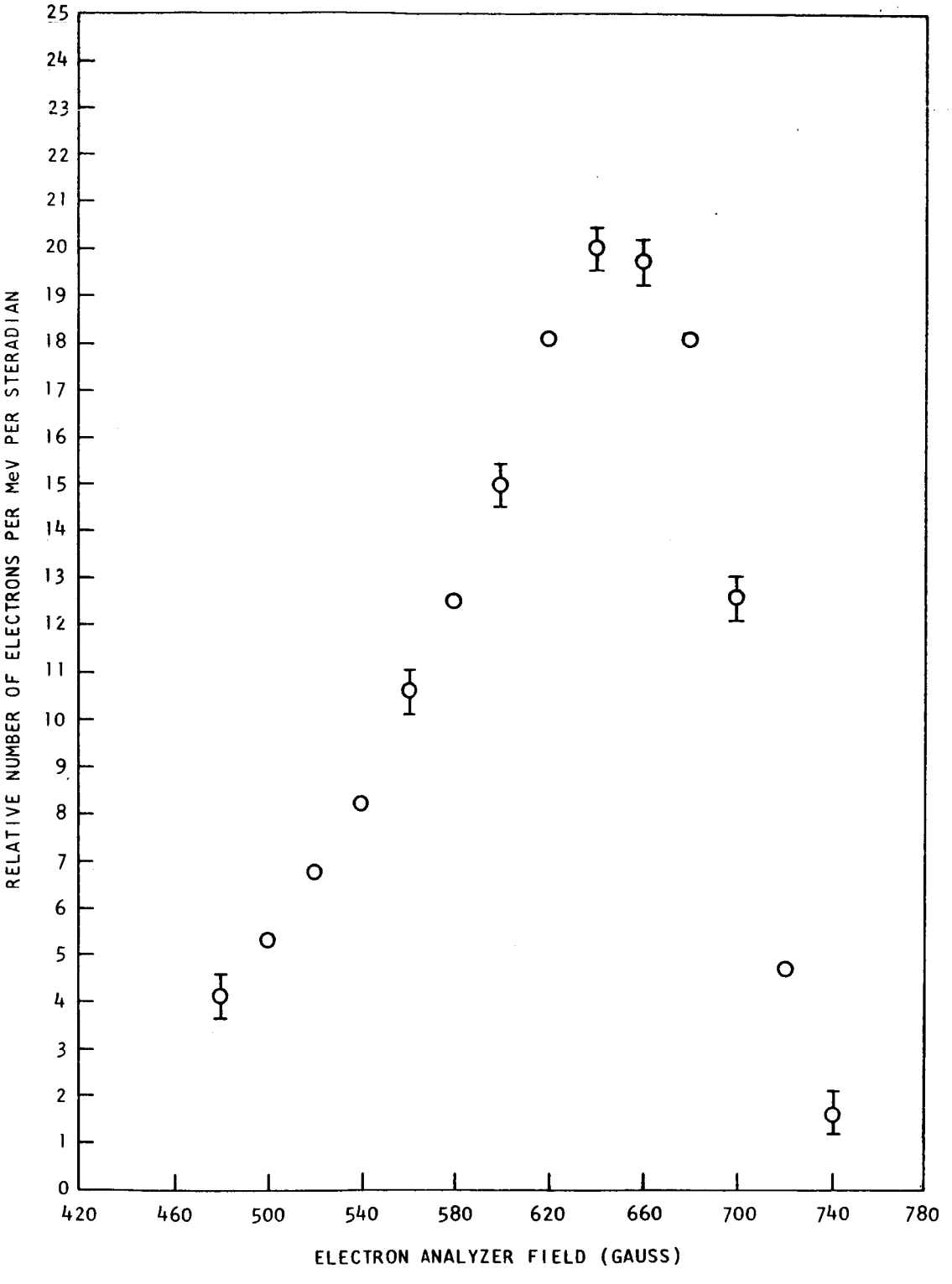

Fig. 27--Electron spectrum obtained at 30 degrees; 8.2 MeV electrons normally incident upon a 2.4 g/cm^2 aluminum target.

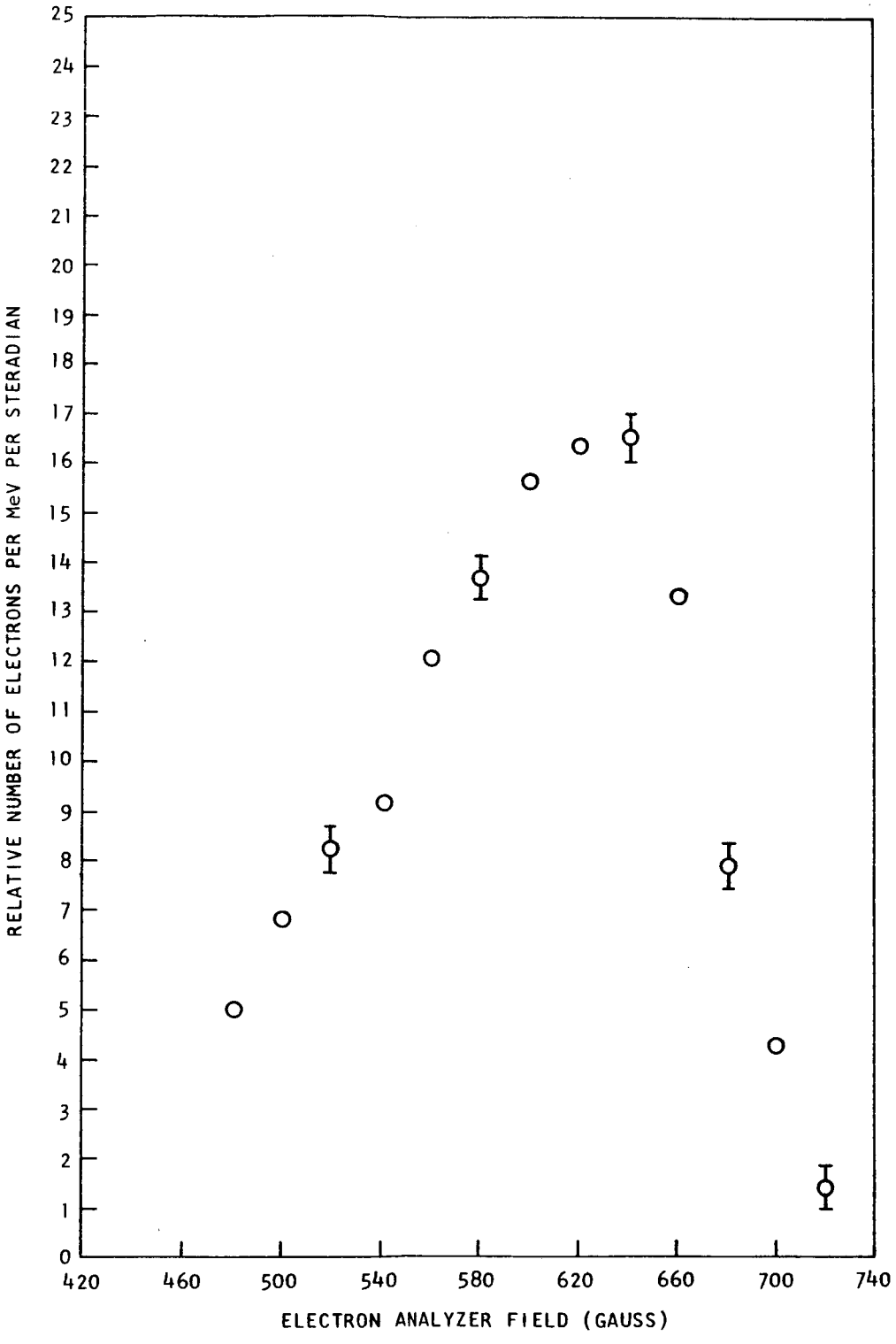

Fig. 28--Electron spectrum obtained at 40 degrees; 8.2 MeV electrons normally incident upon a 2.4 g/cm^2 aluminum target.

A comparison of the FWHM of the 8.2 MeV experimental distributions with that of the 8.0 MeV Monte Carlo distribution indicates that the 8.2 MeV data is consistent with a greater degree of energy straggling than is indicated in the Monte Carlo calculations. On the other hand, the FWHM of the 4.0 MeV straggled electron energy distributions and the 4.0 MeV Monte Carlo calculations are in fair agreement.

A possible explanation of the relative lack of agreement in the case of the 8.0 MeV theoretical and experimental distributions may be that the Monte Carlo program used by Berger does not consider the contributions of bremsstrahlung to the energy straggling. The contribution of bremsstrahlung is more significant at 8.0 MeV than at 4.0 MeV. Further comparisons between experiment and theory are desirable. The use of a large number of case histories in the Monte Carlo calculations as well as an experimental investigation of electron transport in targets whose thickness approaches the range of the electrons would provide material for a more critical comparison between theory and measurement.

VII. RELATIVE ANGULAR DISTRIBUTIONS

7.1 GENERAL DISCUSSION

The present system for monitoring the incident Linac beam (Fig. 3) involves the use of a Faraday cup which is inserted into the beam path in front of the target before and after each data run. Ideally, it is desirable to integrate the beam current at the same time that the spectrometer measurements are being made. (The scattering chamber described in Section IX is designed so that a Faraday cup can be used to integrate the incident beam current concurrently with bremsstrahlung spectrometer and electron spectrometer measurements.) In the present experimental arrangement the NaI(Tl) bremsstrahlung spectrometer is used to monitor the incident beam when the electron spectrometer is being used and vice versa; the relationship between the bremsstrahlung spectrometer counting rate and the magnitude of the incident beam is determined for each different angle, target material, or target thickness.

The experimental arrangement shown in Figs. 2 and 3 allows the maximum angle between the incident Linac electron beam and the emission angle of spectrum observation to be 45 degrees, corresponding to the maximum angular deflection of the bellows. The maximum angle of observation in the case of the new scattering chamber will be 165 degrees.

The Faraday cup, shown in Fig. 3, can be moved up into or out of the beam without turning off the LINAC. The Linac beam remains relatively steady as long as the Linac is not turned off; an alternating set of Faraday

cup current readings and bremsstrahlung spectrometer count readings has been made to determine the relationship of the bremsstrahlung spectrometer counting rate to the incident Linac beam current.

Table 2 lists a typical set of Faraday cup current measurements with corresponding bremsstrahlung spectrometer counting rates. The results shown in Table 1 were obtained at 40 degrees with 8.2 MeV electrons incident on a 2.4 g/cm^2 aluminum target. The average of the five ratios is 2.85×10^{-15} amps x minutes/bremsstrahlung counts. The average target-out bremsstrahlung spectrometer count was approximately 250.

7.2 ANGULAR DISTRIBUTION MEASUREMENTS

Figure 29 shows the angular distribution of electrons obtained for 8.2 MeV electrons incident upon a 2.4-g/cm^2 aluminum target. The error bars are consistent with the spread in Faraday cup current to bremsstrahlung count ratios such as indicated in Table 2 for 40 degrees. The experimental points correspond to the maximum value of the energy distribution. The histogram corresponds to a Monte Carlo calculation by Berger for 1,000 histories of 8 MeV electrons incident on a 2.4 g/cm^2 aluminum target.

The dips in the experimental and the Monte Carlo angular distributions at 0 degrees are within the errors and should not be taken seriously. Berger has made Monte Carlo calculations at other energies which are based on over 10,000 histories. These more accurate Monte Carlo calculations, based on more histories, do not show a dip at 0 degrees.

Figure 30 shows the angular distribution obtained for 4.0 MeV electrons normally incident upon a 1.24-g/cm^2 aluminum target. The histogram corresponds to a Monte Carlo calculation by Berger for 1,000 histories of 4.0 MeV electrons incident on a 1.24-g/cm^2 aluminum target.

VIII. BREMSSTRAHLUNG SPECTROMETER

8.1 GENERAL DISCUSSION

The bremsstrahlung spectrometer consists of a 5 by 6 inch NaI(Tl) crystal in a lead pig. The front side of the pig, i.e., the side facing the target, is 12 inches thick. The other five sides consist of at least 6 inches of lead. A number of lead collimators with different orifices can be easily inserted into the front face of the pig.

The use of the bremsstrahlung spectrometer involves a number of procedures and corrections. The relationship between pulse height and photon energy must be determined. The response of the spectrometer to

Table 2

TYPICAL ABSOLUTE CALIBRATION OF BREMSSTRAHLUNG SPECTROMETER WITH THE FARADAY CUP

Faraday Cup Current (10^{-11} Amps)			
Before Bremsstrahlung Spectrometer Count	After Bremsstrahlung Spectrometer Count	Bremsstrahlung Spectrometer Count in 1 min.	Bremsstrahlung Monitor Calibration
A	B	C	(A+B)/2C
3.25	3.50	10281	3.27×10^{-4}
3.25	3.35	12557	2.62×10^{-4}
3.35	3.40	12745	2.65×10^{-4}
3.45	3.30	11593	2.81×10^{-4}
3.30	3.45	12058	AV = 2.82×10^{-4}

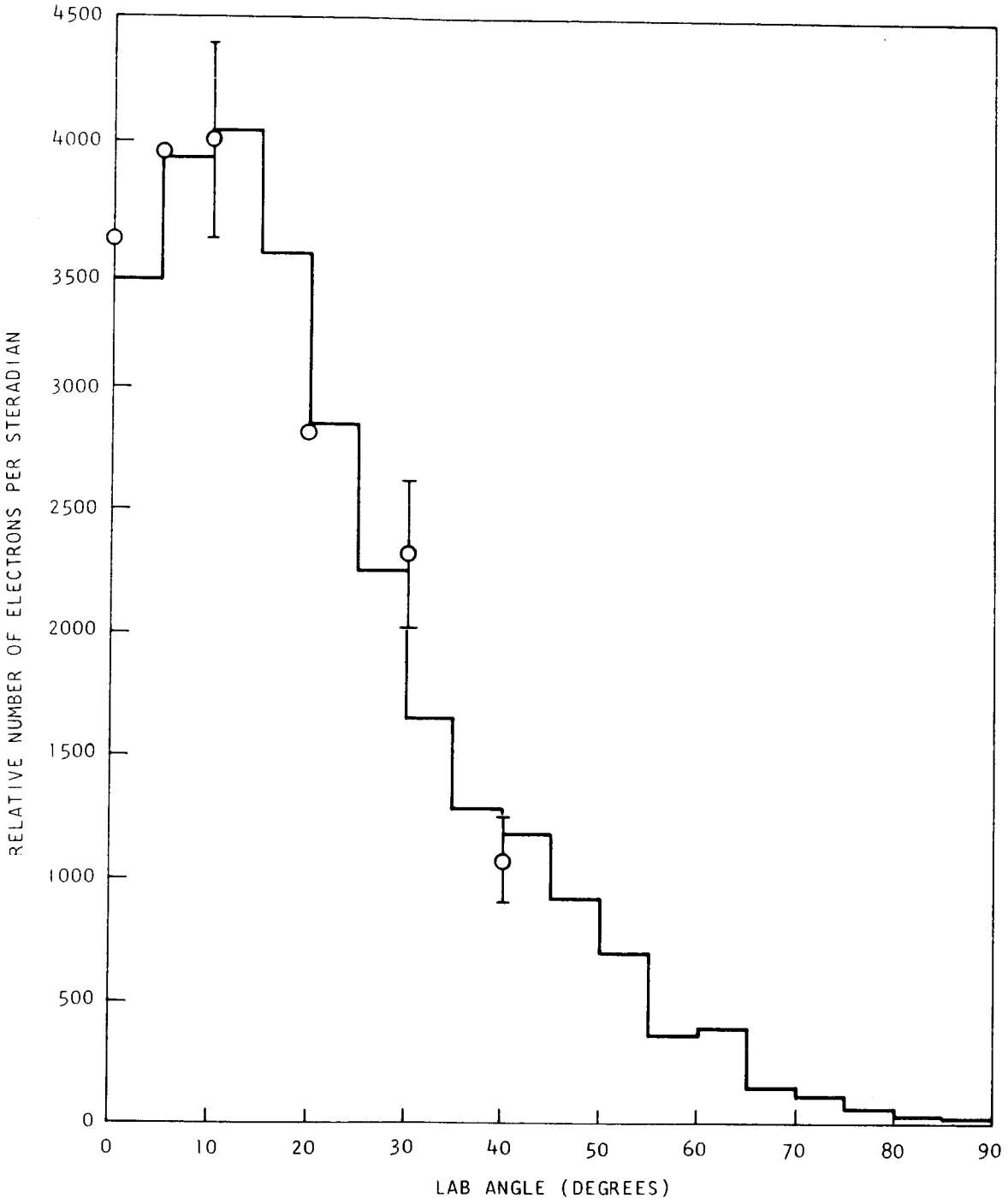

Fig. 29--Electron angular distribution produced by the bombardment of a 2.4 g/cm^2 aluminum target with 8.2 MeV electrons. The histogram corresponds to Berger's Monte Carlo calculation for 8.0 MeV electrons incident upon a 2.4 g/cm^2 aluminum target.

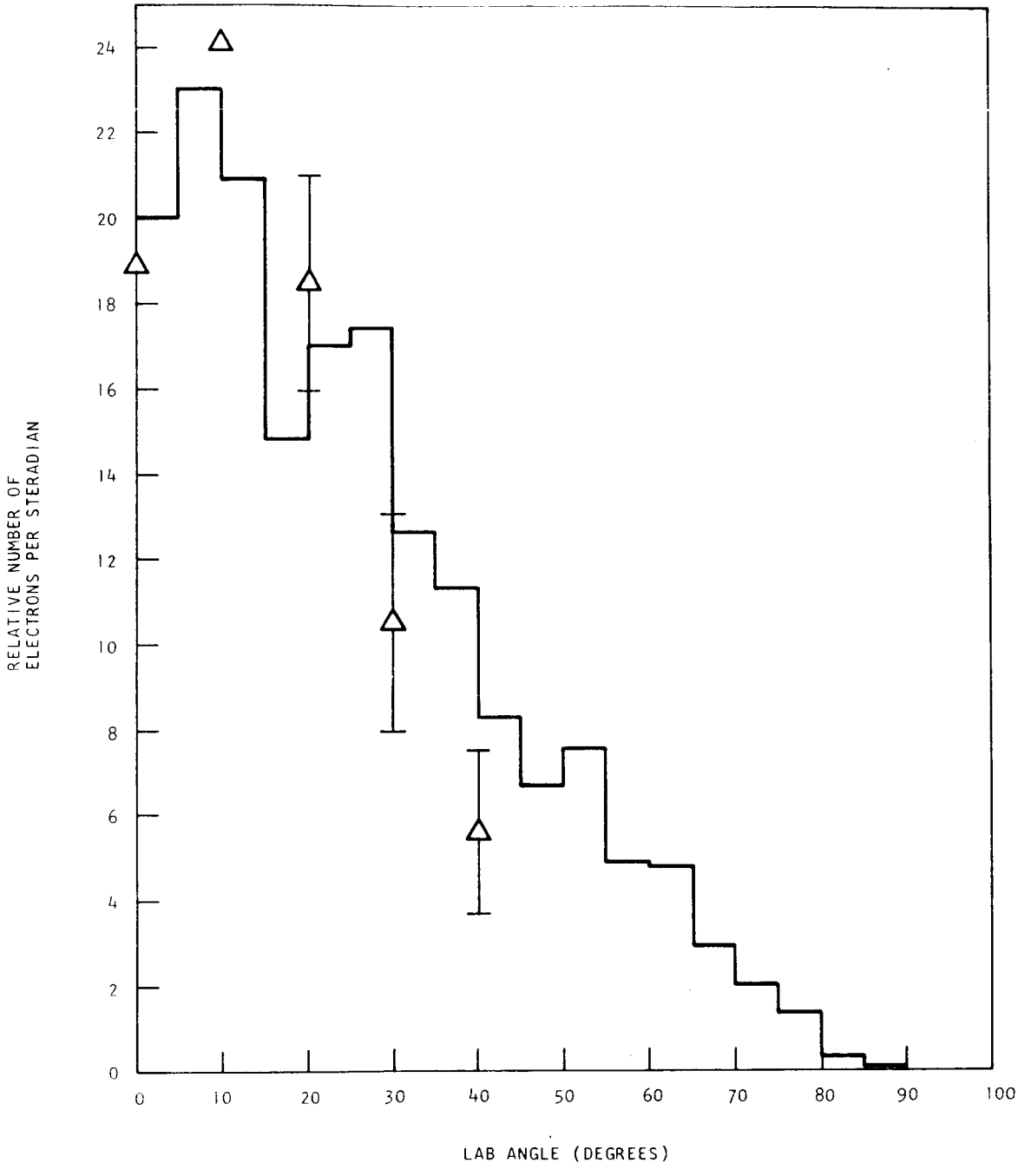

Fig. 30--Electron angular distribution produced by the bombardment of a 1.24 g/cm^2 aluminum target with 4.0 MeV electrons. The histogram corresponds to Berger's Monte Carlo calculation for 4.0 MeV electrons incident upon a 1.24 g/cm^2 aluminum target.

a monochromatic photon spectra must be established in order to determine a set of response functions. After a set of response functions have been determined, the functions can be put into the form of a diagonal matrix. This matrix must then be inverted so that the true bremsstrahlung spectra can be determined from the raw data. Every NaI(Tl) bremsstrahlung spectrometer measurement, whether to determine a response function or a bremsstrahlung spectrum, must be corrected for pulse pile-up. A background counting rate subtraction must also be made for both response function measurements and for bremsstrahlung measurements.

8.2 NaI(Tl) CRYSTAL BREMSSTRAHLUNG COUNTER BACKGROUND

A number of gamma spectra were taken, using thick aluminum and lead targets, in order to obtain a thorough understanding of the magnitude and sources of the background in the NaI(Tl) crystal spectrometer. Pulse height spectra were measured under a variety of operating conditions; namely: (1) Linac beam on, (2) Linac beam off, (3) target in, (4) target out, (5) coincidence gate in coincidence with Linac beam pulse, and (6) coincidence gate delayed 20 μsec after Linac beam pulse. By changing angle and target material the incident electron beam current could be varied over a range of approximately 2,000 to 1. A block diagram of the electronics used in these various measurements is shown in Fig. 31.

The background spectra obtained with the beam off, with the target out, and with the coincidence gate delayed 20 μsec were all essentially the same in shape and magnitude. Moreover, the magnitude of the background spectrum was directly proportional to the length of the gate pulse. The results of this background investigation have demonstrated that the major portion of the gamma background is random in time and not associated with the Linac pulse. The background in the bremsstrahlung NaI(Tl) crystal does not come from the beam collimators or from the vacuum pipes associated with the experimental apparatus. Probable sources of background are nuclear activation of impurities in the lead shielding and other objects in the experimental cell.

Typical bremsstrahlung pulse height spectra measured during this investigation are shown in Figs. 32 through 35. These are all 10-minute runs. Figures 32, 33, and 34 show bremsstrahlung spectra for 8 MeV electrons incident on a 0.35-inch thick aluminum target; photon emission angles are 0°, 10°, and 40° respectively. The associated background spectrum for each run is also shown. Figure 35 shows the results of a similar run for 8 MeV electrons incident on a 0.087-inch lead target; this bremsstrahlung spectrum was obtained at 10°. Depending upon the value of the pulse heights compared, the bremsstrahlung-spectrum-to-background-spectrum ratio varied from 3/1 to 100/1. This bremsstrahlung-to-background ratio will be considerably increased by an improved pulse height

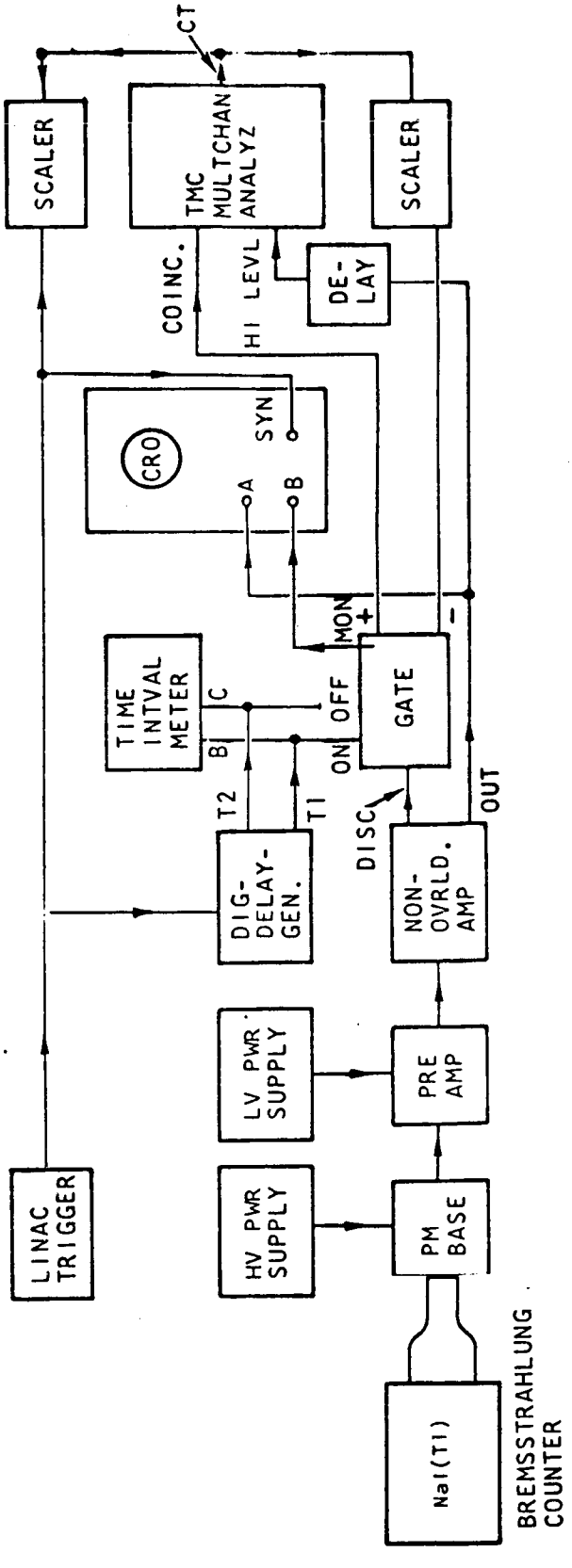

Fig. 31--Block diagram of electronics used in obtaining data shown in Figs. 32 to 34. This diagram is essentially the same as that shown in Fig. 7, except that the bremsstrahlung spectrum is pulse height analyzed.

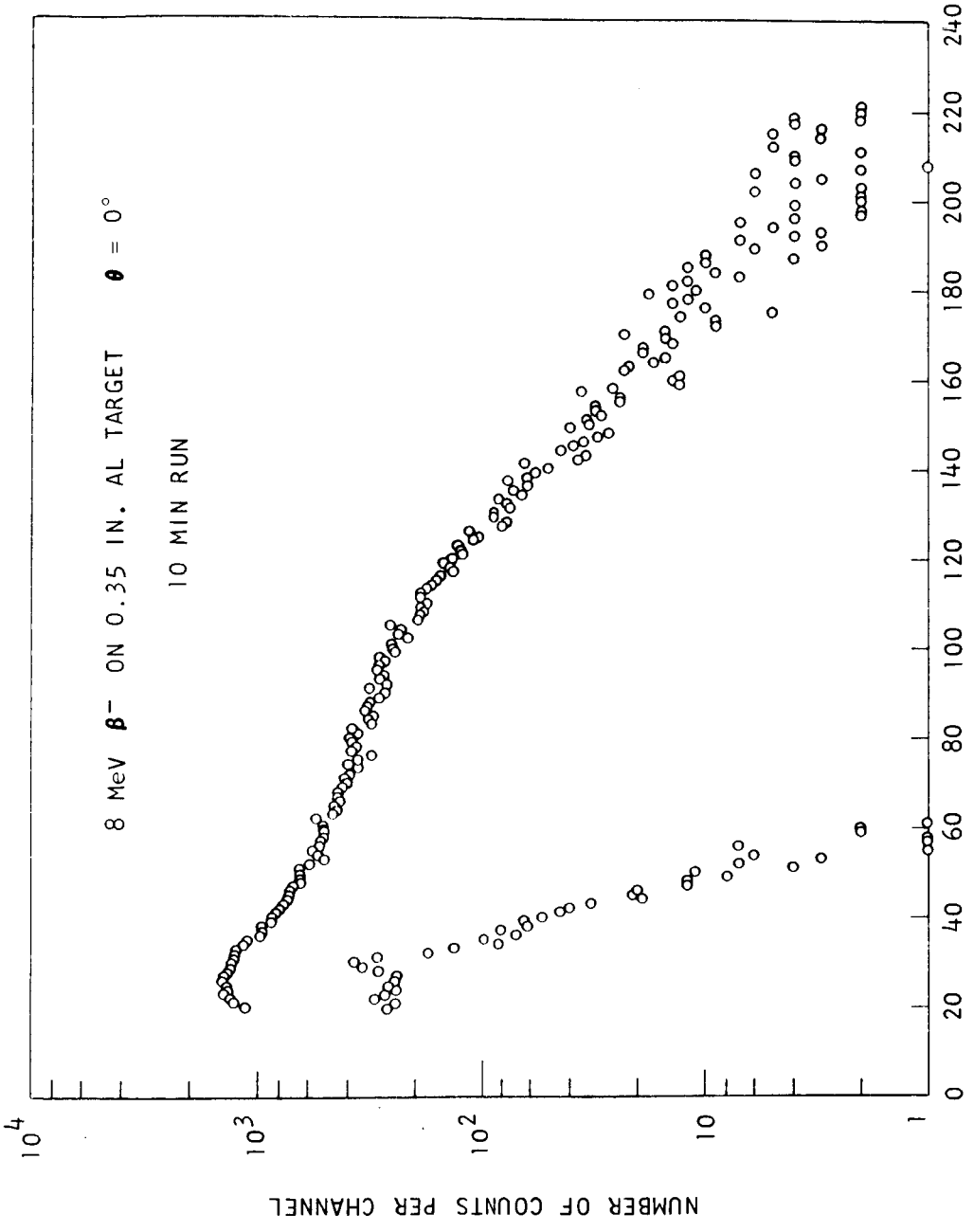

Fig. 32--Bremsstrahlung pulse height spectrum and associated background for 8 MeV electrons incident on a 0.35 inch thick aluminum target. The angle of emission is 0°, the run time is 10 minutes.

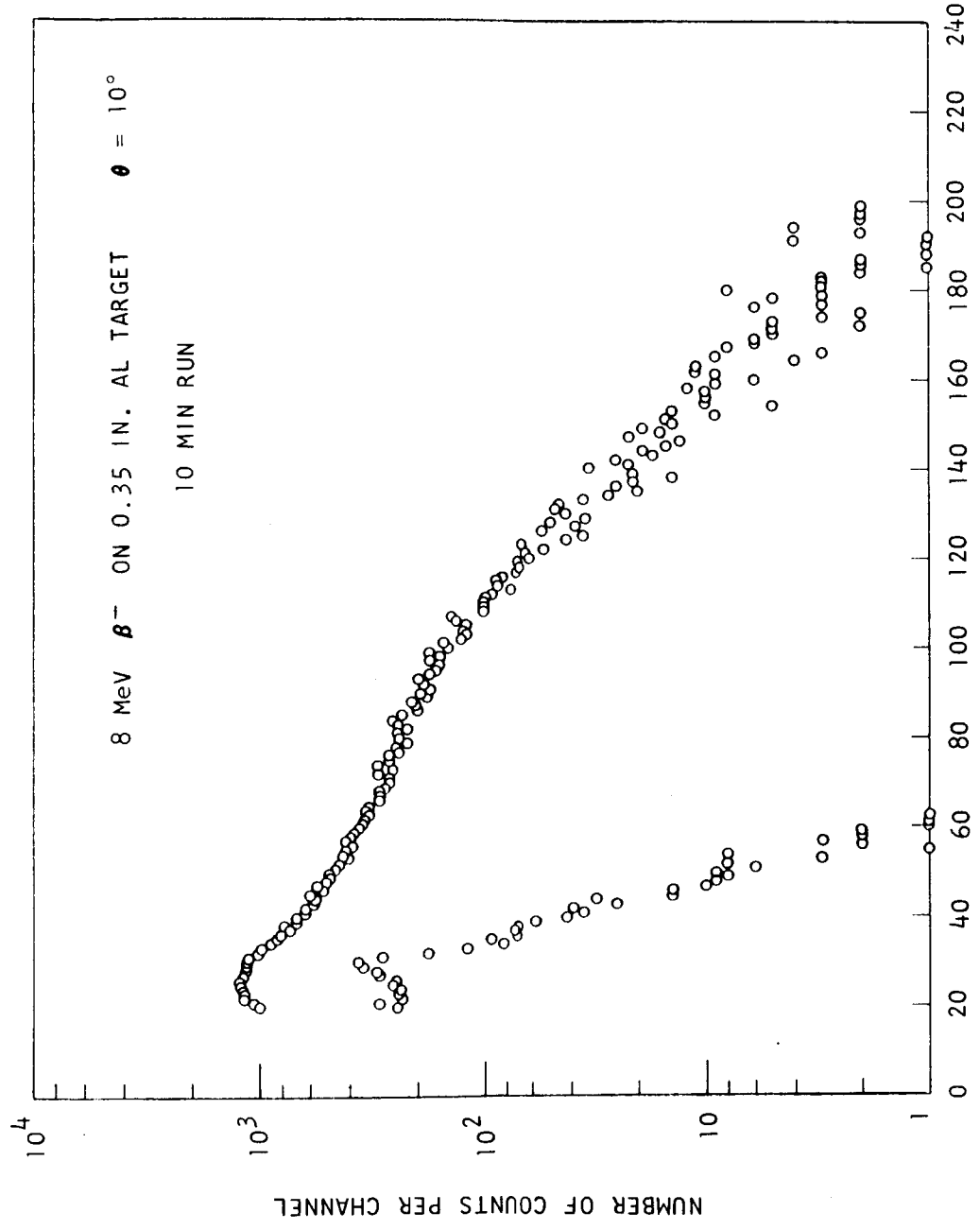

Fig. 33--Bremsstrahlung pulse height spectrum and associated background for 8 MeV electrons incident on a 0.35 inch thick aluminum target. The angle of emission is 10°, the run time is 10 minutes.

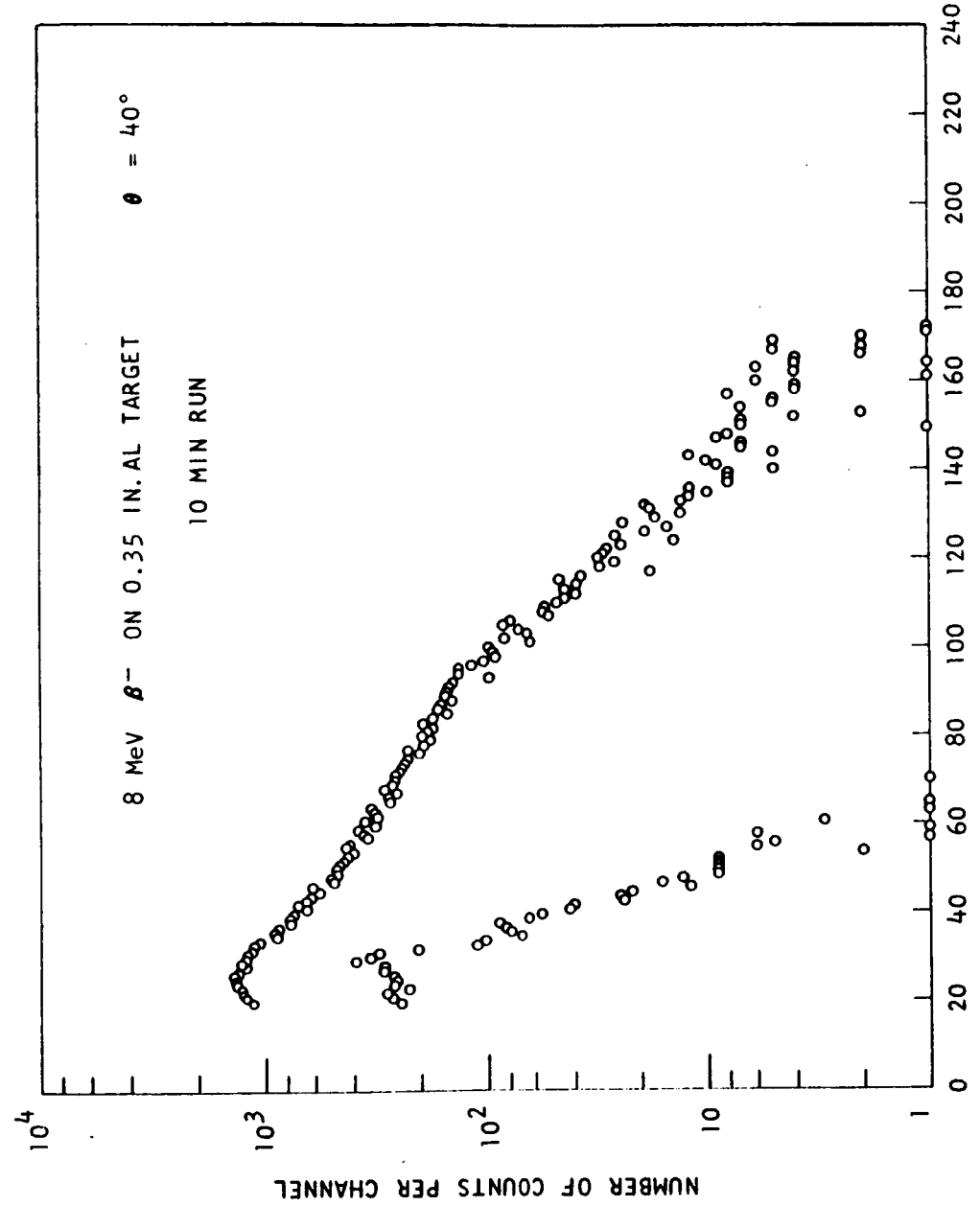

Fig. 34--Bremsstrahlung pulse height spectrum and associated background for 8 MeV electrons incident on a 0.35 inch thick aluminum target. The angle of emission is 40°, the run time is 10 minutes.

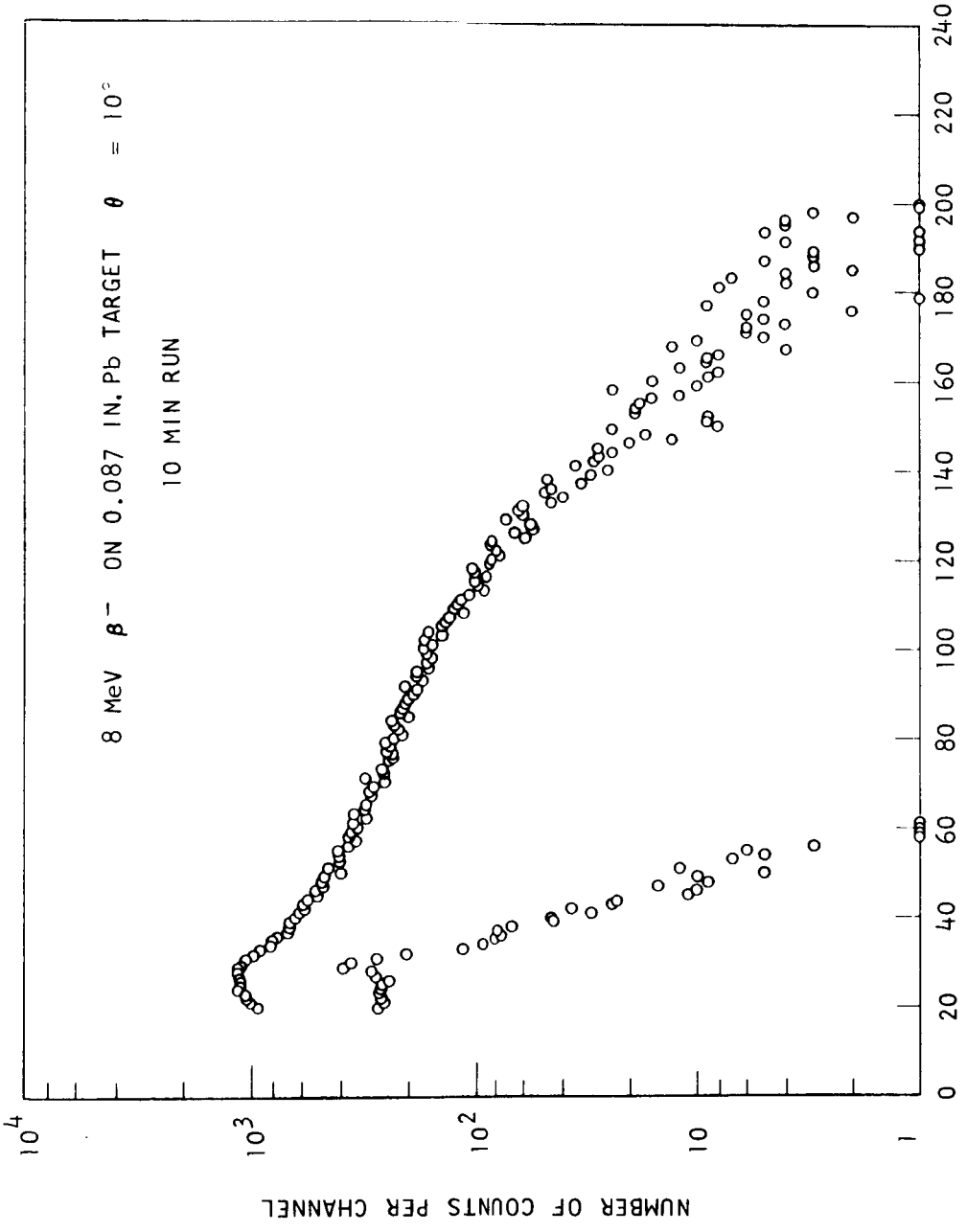

Fig. 35--Bremsstrahlung pulse height spectrum and associated background for 8 MeV electrons incident on a 0.087 inch thick lead target. The angle of emission is 10^{o}, the run time is 10 minutes.

analyzer gating circuit. In the electronics (Fig. 31) used to obtain the data shown in Figs. 32 to 35, pulses from the gamma spectrometer were sampled for 1 μsec every time the Linac beam was pulsed. A 40-nanosecond gate would offer an improvement by a factor of 60.

The improved gating system for the gamma-ray spectrometer is illustrated in Fig. 36. Two linear outputs are taken from the preamplifier; one of which goes directly to the pulse height analyzer input, and another which is fed to the cosmic double delay line amplifier to create a fast gate. The double delay line amplifier differentiates the linear pulse from the gamma detector, producing a baseline crossover which activates the crossover discriminator to give a 50-nanosecond wide pulse with less than a 10-nanosecond jitter from the tunnel diode monostable I. This pulse is placed in coincidence with a similar gate pulse derived from the Linac injector trigger. Only detector pulses which originate during the Linac beam burst are accepted by the tunnel diode "and" circuit. The length of the output of the tunnel diode monostable II may be varied between 40 nanoseconds and 250 nanoseconds to correspond to the length of the Linac beam pulse. If the length of the pulse from the tunnel diode monostable multivibrator is set to 40 nanoseconds, background pulses occuring outside the 40-nanosecond interval will not be analyzed and will not contribute to the background rate.

Figure 37 shows a bremsstrahlung spectrum measurement along with two background spectrum measurements. The triangles correspond to the background obtained with the fast nanosecond electronics and the circles correspond to the background spectrum obtained with the microsecond electronics. Both background measurements correspond to a 20-microsecond delay between the Linac beam burst and the gate pulse.

The microsecond electronics (Fig. 31) yielded a 1-microsecond on-gate time. The nanosecond electronics on-gate time corresponded to 250 nanoseconds. Jitter time in the arrival of the Linac injector pulse prevented a reduction of the on time to less than 250 nanoseconds. The magnitude of the background spectrum could, therefore, be reduced only by a factor of 4. Work is now in progress to reduce the time jitter in the Linac gate pulse. The background counting rate should be reduced by at least another factor of 4 or greater.

8.3 DETERMINATION OF NaI CRYSTAL RESPONSE FUNCTION

The NaI crystal response function can be determined over a wide range of photon energies by using monoenergetic photons from the in-flight annihilation of positrons. The General Atomic Linac has been used to produce positrons in a radiation shower by bombarding a high Z target located

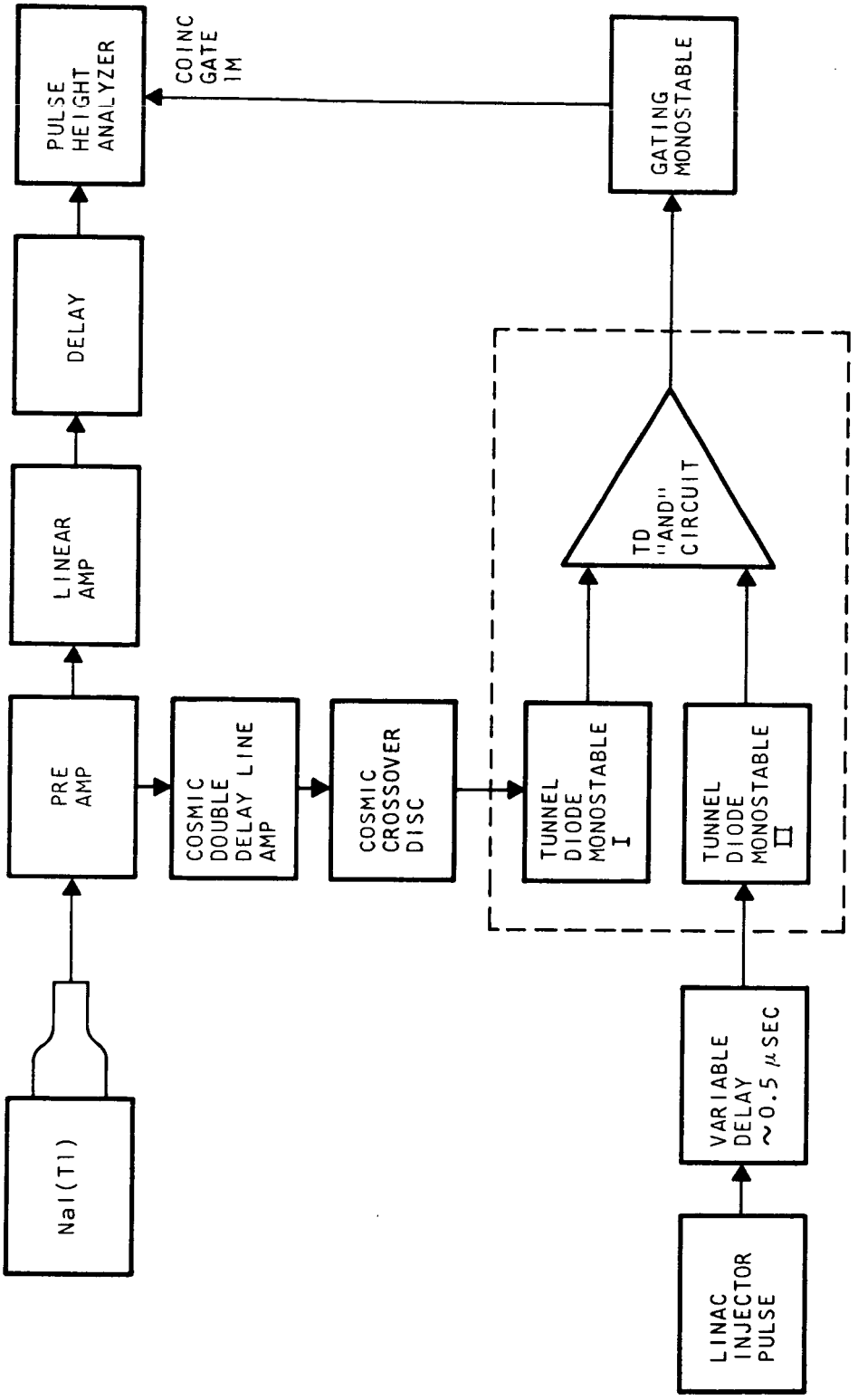

Fig. 36--Improved gating system for the gamma-ray spectrometer

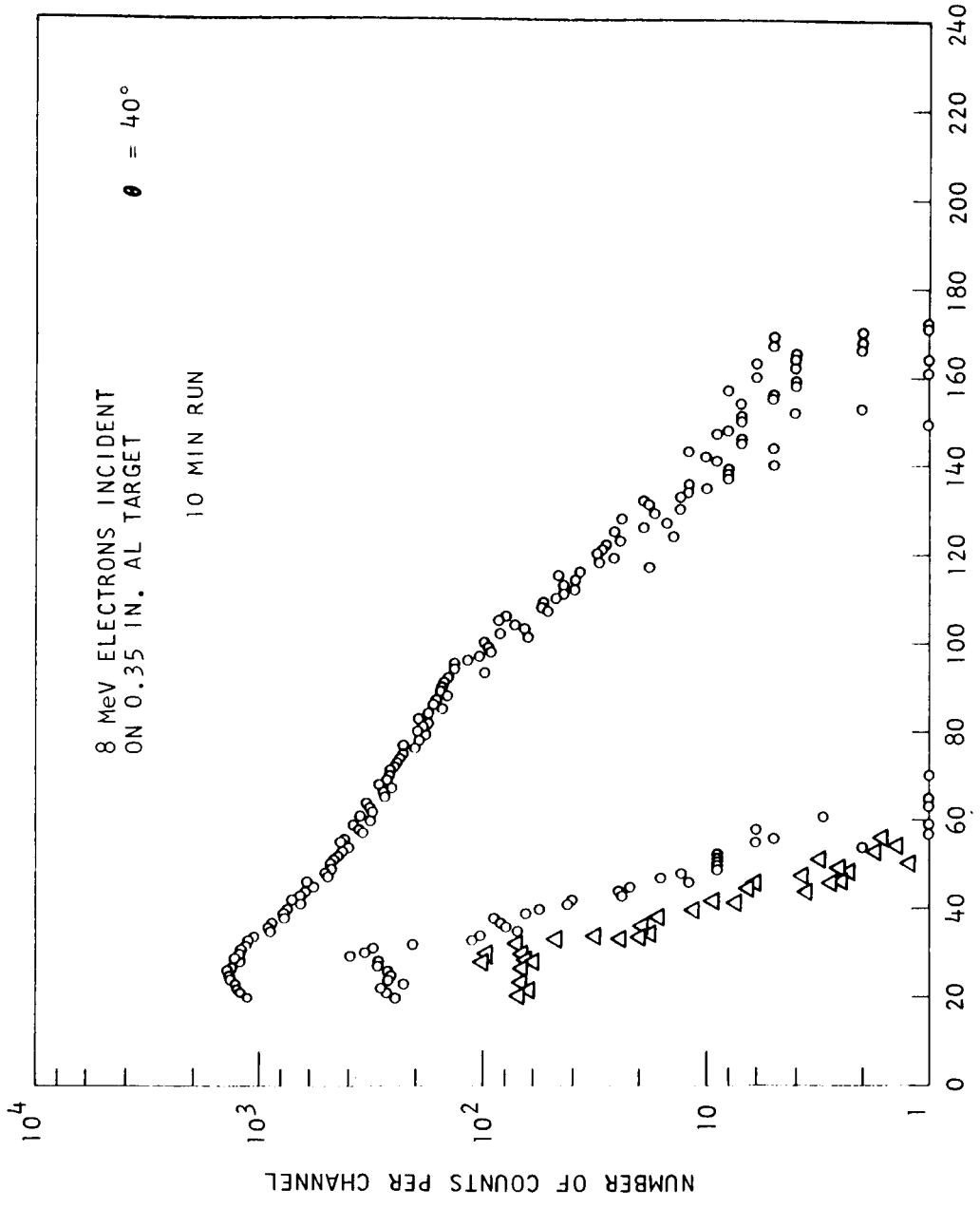

Fig. 37--Bremsstrahlung pulse height spectrum and associated background for 8 MeV electrons incident on a 0.35 inch thick aluminum target. The angle of emission is 40^{o}, the run time is 10 minutes. The circles correspond to the microsecond electronics. The triangles to the fast electronics.

between the first two accelerator sections. Some of the positrons created in pair production processes are then accelerated in the second and third sections of the Linac by adjusting the R. F. power of the last two sections to be 180 degrees out of phase with the first section.[18] The accelerated positrons are magnetically analyzed and allowed to strike a thin beryllium target where some annihilate in flight, producing monoenergetic photons in the forward direction with an energy equal to the positron kinetic energy plus its rest mass.[19] The positrons also produce bremsstrahlung. After passing through the beryllium target the beam can be monitored with a Faraday cup placed at the position of the electron analyzer energy detector shown in Fig. 2.

The contribution to the positron spectrum by positron bremsstrahlung can be ascertained by bombarding the same beryllium target with electrons of the same energy, since the bremsstrahlung cross sections are the same for both positrons and electrons in the MeV range.

Figure 38 illustrates two measured pulse height spectra: (1) the spectrum from the bremsstrahlung plus annihilation radiation produced by 8 MeV positrons, and (2) the spectrum from the bremsstrahlung produced by 8 MeV electrons. The background has been subtracted from both spectra. However, no pile-up subtraction was made. Figure 39 shows the response function for 8 MeV photons obtained by subtracting the electron bremsstrahlung spectrum from the positron distribution. The high energy tail is presumably the result of pulse pile-up. Figure 40 shows similar pulse height spectra produced with 6 MeV positrons and 6 MeV electrons. Figure 41 is the response function for 6 MeV photons.

8.4 PILE-UP CORRECTIONS

Starfelt and Koch[20] give a recipe for subtracting the double pulses from a measured spectrum. The spectrum of double pulses is given by

$$P''(\epsilon) = p \frac{\int_0^{\epsilon} P(\epsilon_i)\, P(\epsilon - \epsilon_i)\, d\epsilon_i}{\int_0^{\epsilon_{max}} P(\epsilon_i)\, d\epsilon_i} \qquad (3)$$

where $P(\epsilon_i)$ is a spectrum of single pulses and p is the ratio of the probability of recording two photons in the same Linac burst to the probability of recording one photon. $P''(\epsilon)$ can be calculated by successive approximations. Equation (3) is based on the simple addition of pulses during a Linac pulse.

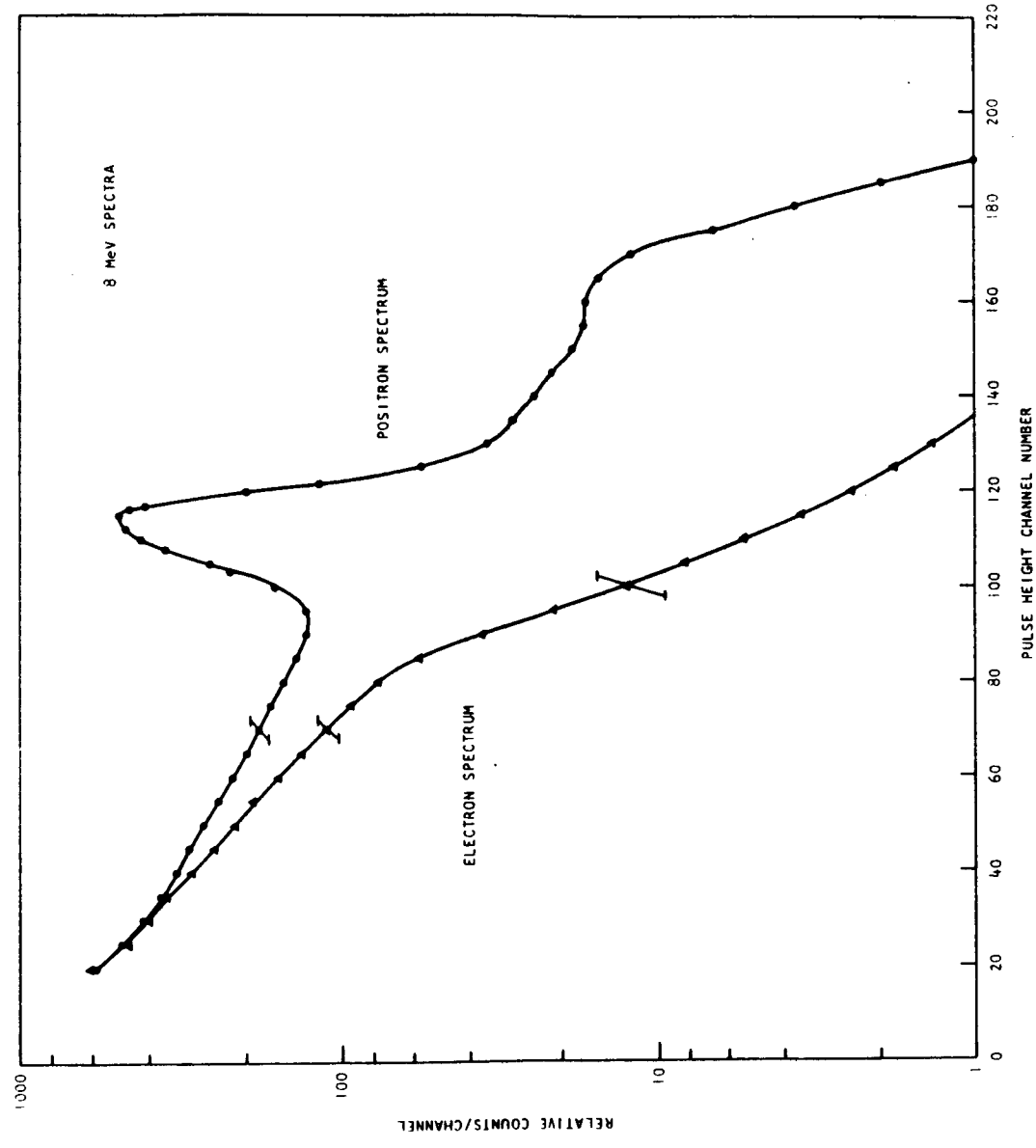

Fig. 38--Spectra produced by 8 MeV electron and positron bombardment of a beryllium target 10 mills thick. The electron spectrum consists of bremsstrahlung. The positron spectrum consists of both bremsstrahlung and annihilation radiation.

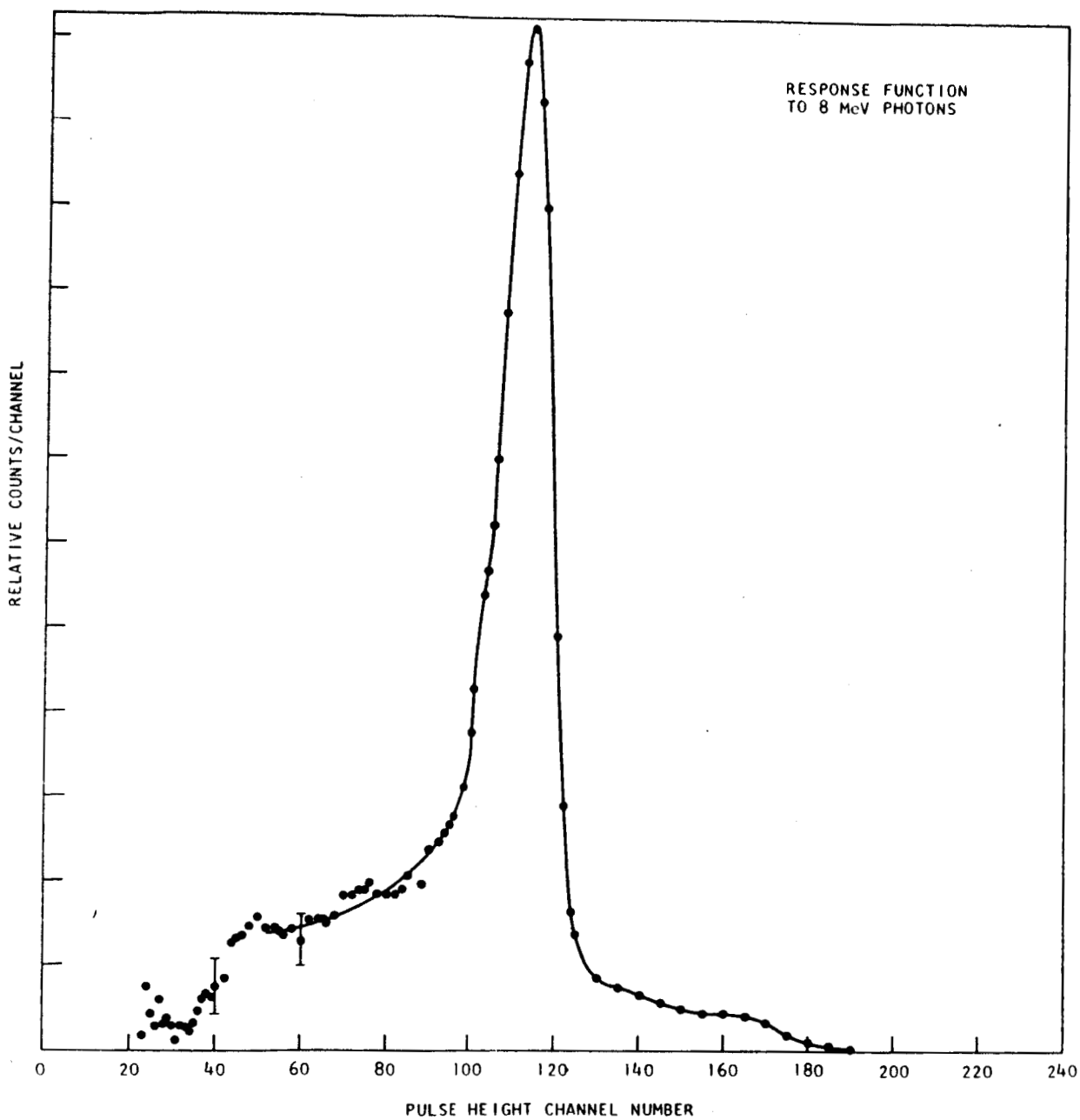

Fig. 39--Response function of the 5 in. by 6 in. NaI(Tl) crystal to 8 MeV photons. The response function was obtained by subtracting the electron spectrum from the positron spectrum shown in Fig. 1.

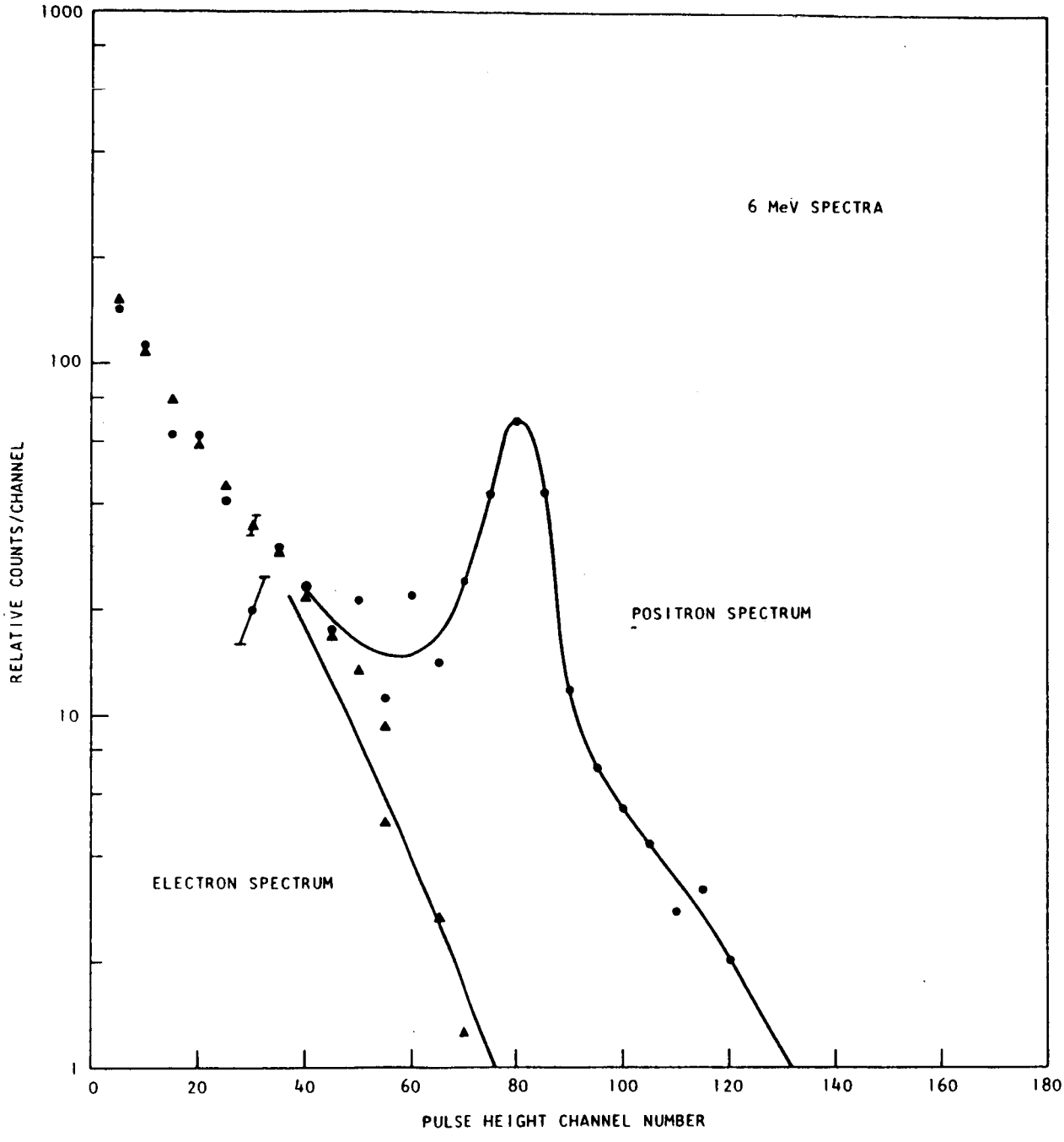

Fig. 40--Spectra produced by 6 MeV electron and positron bombardment of a 10 mill thick beryllium target. The electron spectrum consists of bremsstrahlung. The positron spectrum consists of both bremsstrahlung and annihilation radiation.

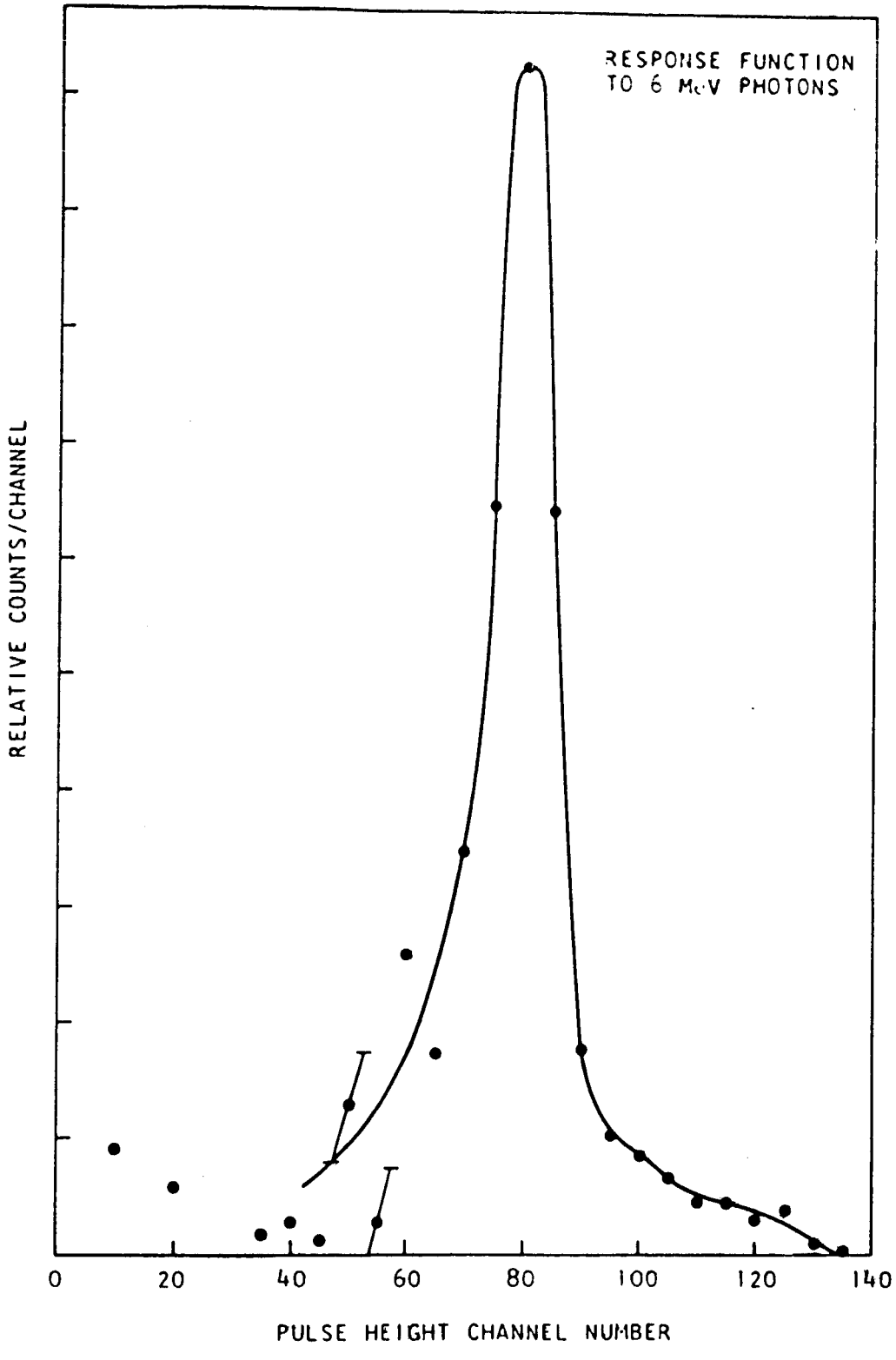

Fig. 41--Response function of the 5 in. by 6 in. NaI(Tl) crystal to 6 MeV photons. The response function was obtained by subtracting the electron spectrum from the positron spectrum shown in Fig. 3.

8.5 RESPONSE FUNCTION INVERSION

The actual bremsstrahlung photon spectrum N_i is computed from the spectrometer pulse height spectrum P_j by

$$N_i = \sum_{j=1}^{n} m_{ij}^{-1} P_j$$

where m_{ij} is the response function matrix for the spectrometer and i and j refer to photon energy bins and voltage pulse height bins, respectively.[21-24] The matrix m_{ij} will be constructed from response function data resulting from more refined measurements using both radioactive sources and monoenergetic photons from positron annihilation.

IX. DESIGN OF STRIP SEALED CONTINUOUS ROTATION SCATTERING CHAMBER

The problem of designing a vacuum chamber, with two ports, which can continuously change the angle subtended by their center lines over a wide range, while still maintaining a good vacuum has, fortunately, been considered by a number of experimenters. The scattering chamber described here follows the general design outlined by Hawrylak, Cline, and Grube[25] of the University of Rochester Department of Physics and Astronomy. Figures 42 and 43 depict in a very simplified form the essential ideas contained in the strip-sealed continuous rotation scattering chamber.

Figure 42 presents a top view diagram of the scattering chamber proper together with the sliding stainless steel strip. The sliding strip covers a 1.5 inch slot in the median plane of the chamber. The essentials of the vacuum seal between the slot in the chamber and the flexible stainless steel strip are shown in Fig. 43. Figures 44 and 45 are more detailed plans of the scattering chamber and accompanying equipment. A very important feature of the design is a decoupling arrangement which decouples any forces on the table from the vacuum seal. The forces exerted on the table by two tons of lead shielding can be considerable; the decoupling is absolutely necessary because of the very close tolerances in the vacuum seal. As shown in Fig. 42 the scattering chamber has two beam entrance ports. When the chamber is rotated so that the beam enters the auxiliary beam entrance port, the Bremsstrahlung and straggled electron spectra can be measured at angles from 0 to 140 degrees. On the other hand, when the beam enters the regular beam port, spectra can be measured from 20 to 165 degrees. In this normal position the exit port serves as a beam dumping or "get lost" pipe. The beam dumping pipe serves to

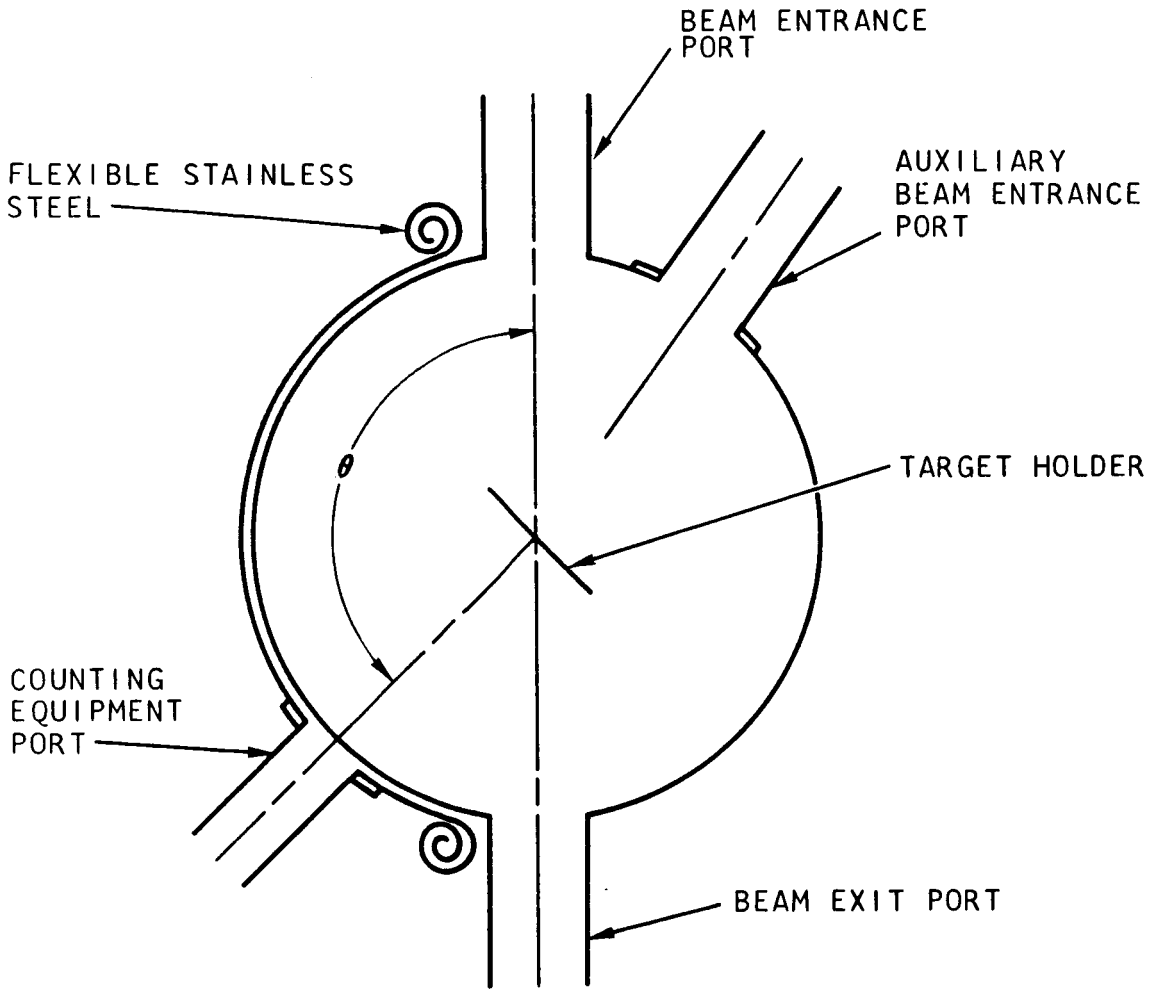

Fig. 42--Top view diagram of scattering chamber

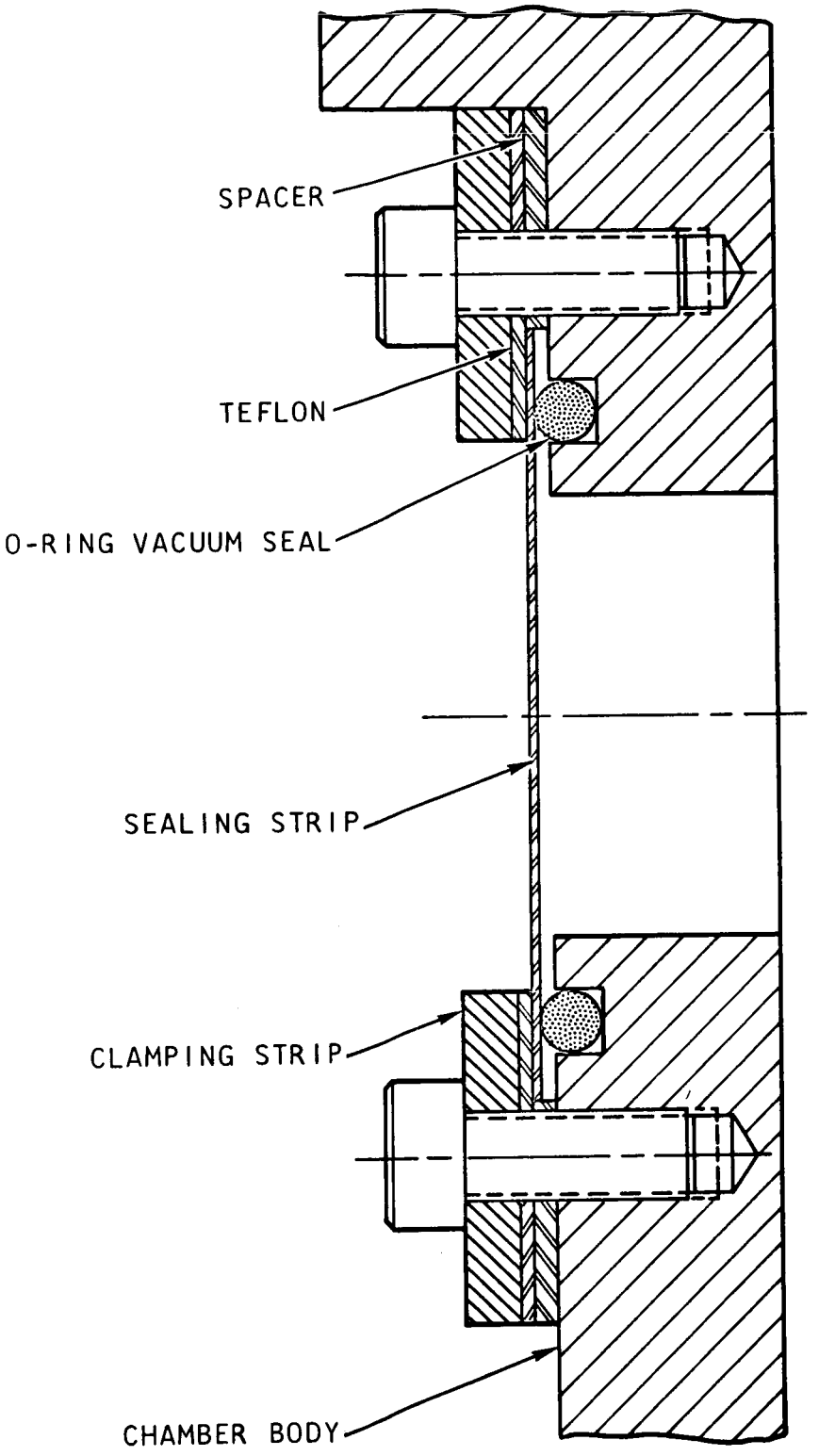

Fig. 43--Diagram of flexible strip vacuum seal

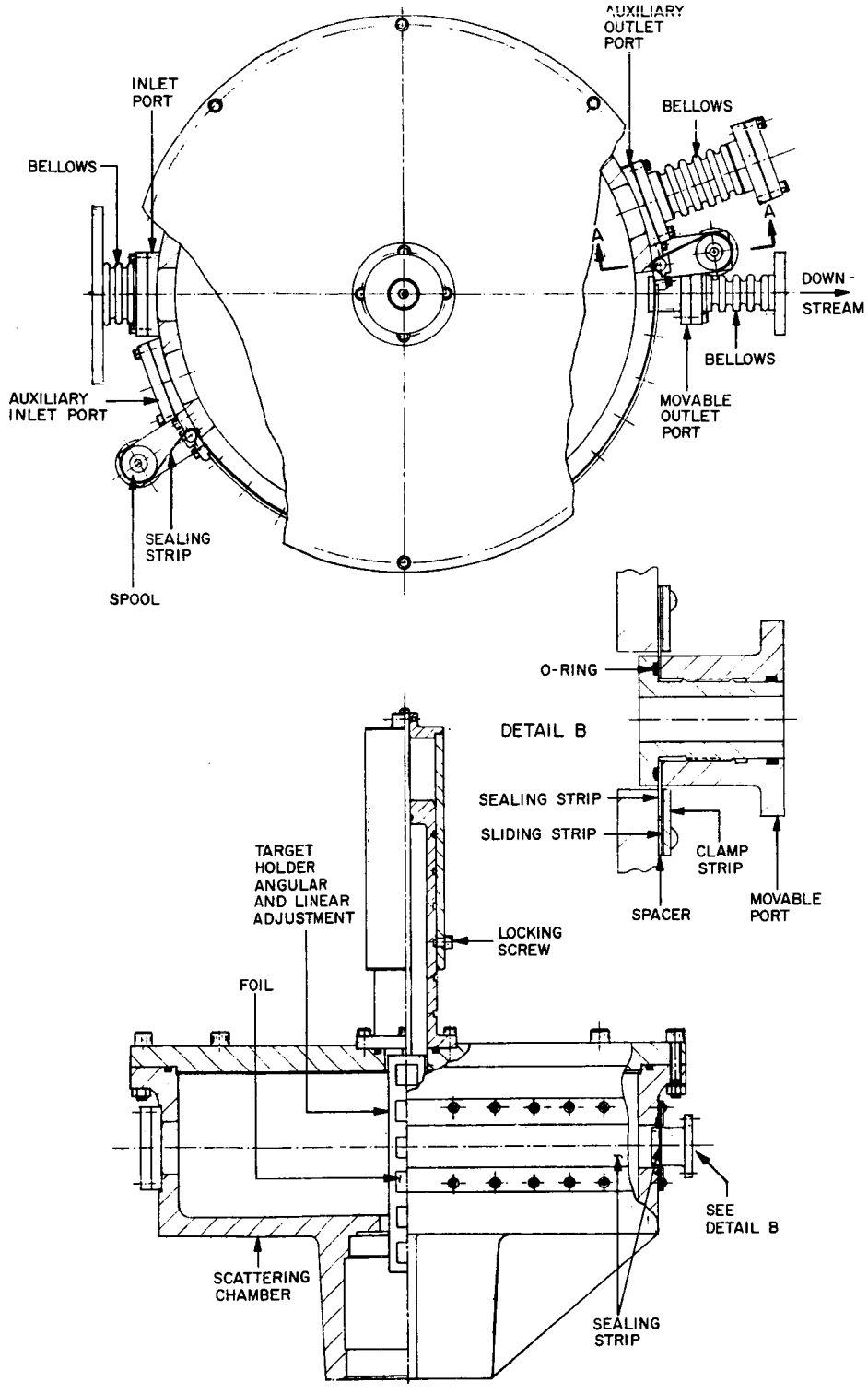

Fig. 44--Detail drawing of scattering chamber

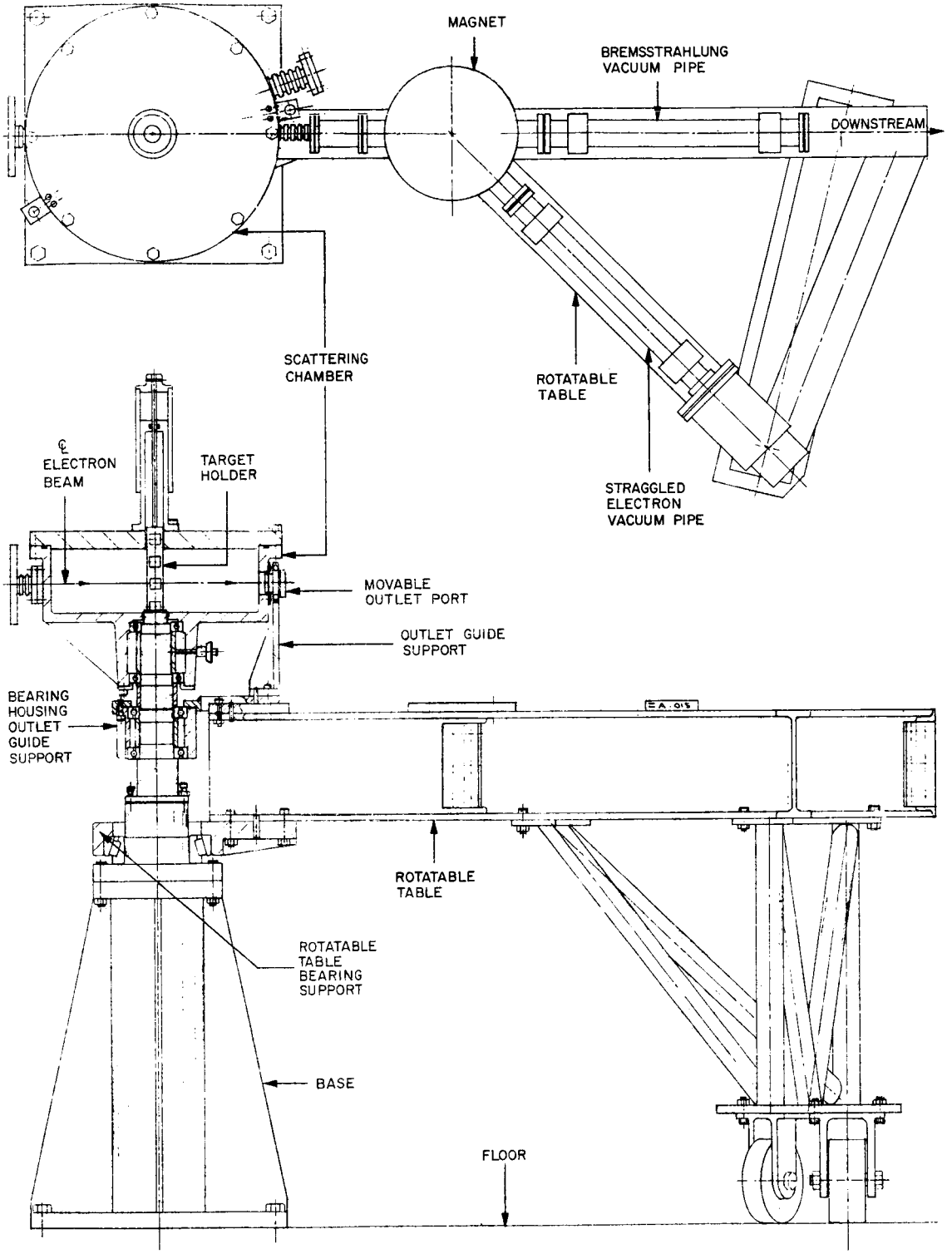

Fig. 45--Detail drawing of scattering chamber plus rotatable detector support assembly

remove the transmitted beam from the vicinity of the bremsstrahlung and electron spectrometers and therefore reduces background.

A Faraday cup or a NaI(Tl) crystal can be positioned at the exit port to monitor the incident beam when the beam enters either the normal or the auxiliary port. Therefore, the beam can be monitored while the electron or bremsstrahlung spectrometer measurements are being made.

XI. CONCLUSIONS

Straggled electron spectra have been measured for various aluminum absorber thicknesses (0.1, 0.2 and 0.5 times the range), angles of emission (0^{o}, 10^{o}, 20^{o}, 30^{o} and 40^{o}), and incident electron energies (8.2 and 4.0 MeV). The experimentally determined spectra have been compared with the results of Berger's Monte Carlo calculations. (See Figs. 13 to 26 and 29 and 30.) The most significant difference between the measurements and the Monte Carlo calculations is that the measurements give a spectrum of greater width. The broader experimental results are to be expected since straggling due to bremsstrahlung was not taken into account in Berger's calculations; however, there may be other causes which contribute to this discrepancy.

The straggling measurements will be refined to remove possible systematic and statistical errors. The reliability of the analyzing magnets used in making the experimental measurements has been improved since the measurements were made. The gaussmeters have also been debugged to yield greater accuracy and reliability. The absolute accuracy of the energy determinations during the straggling measurements reported in this report was ± 2.0%. This accuracy has been improved to ± 0.5%.

Berger has indicated that his straggling calculations will be refined by the inclusion of energy straggling due to the production of bremsstrahlung. Berger's histograms shown in Figs. 13 to 26, 29 and 30 were not calculated in a manner which considered energy straggling arising from the production of bremsstrahlung. The straggling calculations can also be improved by increasing the number of electron histories from 1,000 to 10,000 or more.

Preliminary bremsstrahlung measurements have also been obtained. The results are shown in Figs. 32 to 37. Until now, the emphasis in the bremsstrahlung measurements has been on refining the experimental technique. An effort has been made to obtain the highest ratio of counting-rate-to-background by determining and removing as many sources of background as possible. The following work has been accomplished:

1. A program for calculating the magnitude of the pulse pileup contribution to the measured bremsstrahlung spectra has been developed,

2. the response function of the NaI crystal has been determined for a number of gamma ray energies,

3. a suitable computer program for applying the NaI crystal response function to the raw data in order to obtain the actual bremsstrahlung spectra has also been developed, and

4. work has progressed on developing a fast coincidence circuit that will result in faster and more efficient counting rates in making bremsstrahlung measurements.

The emphasis during this first twelve-month period has been on the design, construction, and accumulation of the apparatus necessary to make experimental measurements. An important portion of the effort has also been directed to debugging the various parts of the experimental apparatus.

The experimental measurements made so far indicate that many more interesting thick target measurements can be made. The results of these measurements would subject existing and future theory and calculational procedures on the passage of electrons through matter to severe experimental tests by varying a large number of significant parameters. For example, the incident electron energies can be varied and the target slab thickness can be varied. Azimuthal dependencies can be studied by changing the angle between the surface of the target slab and the direction of the bombarding electron from 90 degrees to some other angle. Target slab material can be varied over a large range of atomic numbers. The measured straggling spectra can be measured from 0 to 180 degrees. The present experimental setup limits our experimental measurements to from 0 to 45 degrees - this limitation will soon be removed.

Work has progressed on the design of a scattering chamber which will enable thin target, single interaction cross section measurements, and thick target measurements to be made from 0 to 165 degrees. The new scattering chamber will also allow thin target and thick target bremsstrahlung measurements from 0 to 165 degrees.

Thin target, single interaction cross sections are of the utmost importance because they form the basis for any thick target calculation whether the calculation is based on a combination of transport theoretical and Monte Carlo techniques such as are being used by Berger or on a purely transport theoretical approach such as is being actively pursued by R. Scalettar.

ACKNOWLEDGEMENTS

The work described in this report was done with the assistance of W. Brouwer, G. Houghton, W. Hunter, and J. Parez. We would also like to acknowledge the continuing encouragement of J. R. Beyster and E. Haddad and the cooperation of the Linac operators. The discussions with Martin J. Berger and R. Scalettar in regard to the theoretical aspects of the work were very helpful.

REFERENCES

1. W. Bothe, Handbuch der Physik, (H. Geiger, ed.) Vol. 22, 2d ed. p. 1.

2. B. Rossi, High Energy Particles, Prentice-Hall, Englewood Cliffs, New Jersey, (1952).

3. R. D. Birkhoff, Handbuch der Physik, (S. Fugge, ed.), Vol. 34, p. 53, Springer, Berlin, (1958).

4. S. Goudsmit and J. L. Saunderson, Phys. Rev. 57, 24 (1940).

5. L. Landau, J. Phys. USSR 8, 201 (1944).

6. G. Moliere, Z. Nuturforschung, 2a, 133 (1947).

7. G. Moliere, Z. Nuturforschung, 3a, 78 (1948).

8. O. Blunk and S. Leisegang, Z. Physik, 128 (500) (1950).

9. H. A. Bethe, M. E. Rose and L. P. Smith, Proc. Am. Phil. Soc., 78, 573 (1938).

10. H. W. Lewis, Phys. Rev. 78, 526 (1950).

11. E. L. Spencer, Phys. Rev. 98, 1507 (1955).

12. Martin J. Berger, Methods in Computational Physics, Vol. 1, edited by B. Alder, S. Fernbach and M. Rotenberg, Academic Press (1963).

13. K. L. Brown, "Achromatic Beam Translation System for Linear Accelerators", Rev. Sci. Instr. 27, No. 12, 959, (1956).

14. "The focusing properties of a sectional magnetic field for the case of normal entry and exit" are discussed by K. T. Bainbridge in Experimental Nuclear Physics, Vol. 1, edited by E. Segre, John Wiley and Sons, New York and London. The more complicated and general case of non-normal entry and exit is very thoroughly discussed by L. Cartan, J. Phys. Radium, 8, 453, (1937).

15. Val J. Ashby and Henry C. Catron, "Tables of Nuclear Reaction Q Values", U.C.R.L. 5419, February 10, 1959.

16. D. Strominger, J. M. Hollander and G. T. Seaborg, "Table of Isotopes", Rev. Mod. Phys. 30, No. 2, Part II, April 1958.

17. We are indebted to Martin J. Berger for allowing us to use his preliminary 4.0 and 8.0 MeV electron Monte Carlo calculations.

18. R. E. Sund, R. B. Walton, N. J. Noris and M. H. MacGregor, "Positron Yield from a 45-MeV L-Band Linear Accelerator", Nuc. Instr. and Meth. 27, pp. 109-121, (1964).

19 C. P. Jupiter, N. E. Hansen, R. E. Shafer and S. C. Fultz, "Radiations from High Energy Positrons Incident on a Be Target", Phys. Rev. 121, 866, (1961).

20. N. Starfelt and H. W. Koch, "Differential Cross Section Measurements of Thin-target Bremsstrahlung Produced by 2.7 to 9.7 MeV Electrons", Phys. Rev. 102, (1958, 1956).

21. J. Kockum and N. Starfelt, "The Response to High-Energy Gamma Rays of a NaI(Tl) Scintillation Spectrometer", Nucl. Instr. and Meth. 4, 171, (1959).

22. J. H. Hubble, "Response of a Large NaI Detector to High Energy X-Rays", Rev. Sci. Instr. 29, 65, (1958).

23. R. E. Rand, "The Analysis of Continuous Spectra Using the Matrix Method", Nucl. Instr. and Meth. 17, 65, (1962).

24. R. E. Rand, "A Correction to 'The Analysis of Continuous Spectra Using the Matrix Method' ", Nucl. Instr. and Meth. 24, 127, (1963).

25. R. A. Hawrylak, D. Cline and D. F. Grube, to be published in Nucl. Instr. and Meth.